

# Control of complex lithofacies on the shale oil potential in ancient alkaline lacustrine basins: The Fengcheng Formation, Mahu Sag, Junggar basin

Jiahao Lv<sup>a,b</sup>, Fujie Jiang<sup>a,b,\*</sup>, Tao Hu<sup>a,b</sup>, Chenxi Zhang<sup>a,b</sup>, Renda Huang<sup>a,b</sup>, Meiling Hu<sup>a,b</sup>, Jing Xue<sup>a,b</sup>, Liliang Huang<sup>c</sup>, Yuping Wu<sup>a,b</sup>

<sup>a</sup> State Key Laboratory of Petroleum Resources and Prospecting, China University of Petroleum, Beijing, 102249, China

<sup>b</sup> College of Geosciences, China University of Petroleum, Beijing, 102249, China

<sup>c</sup> Research Institute of Exploration and Development, PetroChina Xinjiang Oilfield Company, Karamay, 834000, China

## ARTICLE INFO

### Keywords:

Complex lithofacies  
Shale oil potential  
Fengcheng formation  
Mahu sag  
Alkaline lacustrine basin

## ABSTRACT

The study of ultra-deep (>4500 m) oil and gas reservoirs in hydrocarbon-bearing basins is a hot spot for oil and gas exploration in the world today, the heterogeneity of lithofacies is a key factor influencing the potential of deep-buried shale oil. It is highly important to better understand the control of complex rock on the shale oil potential for shale oil exploration and development. The Fengcheng Formation (P<sub>1</sub>f) in the Mahu Sag is a type of ancient alkaline lacustrine shale oil, which was chosen as a research example in this paper. Four lithofacies were identified based on mineralogy: felsic, lime, dolomitic and mixed shale lithofacies. P<sub>1</sub>f exhibits a very high shale oil potential, and the oil saturation index (OSI) can reach 176 mg HC/g TOC, far exceeding the lower limit of effective benefits. The shale lithofacies of P<sub>1</sub>f is complex, and the complex lithofacies has a controlling effect on shale oil potential, specifically in terms of hydrocarbon generation, storage and hydrocarbon migration. The different lithofacies differ in various aspects and are controlled by different factors. Felsic shale is an enriched oil shale with a high hydrocarbon generation potential and high storage capacity that can receive foreign hydrocarbons. Mixed shale is a self-generating and self-accumulating oil shale with a low hydrocarbon production potential and low storage capacity. Lime shale is a partial reservoir-type oil shale with a low hydrocarbon production capacity and satisfactory storage capacity that can receive foreign hydrocarbons. Dolomite shale is a partial source rock-type oil shale exhibiting a high hydrocarbon generation capacity and low storage capacity, which can expel hydrocarbons. Studies have indicated that felsic shale exhibits a notable hydrocarbon generation potential, high storage capacity, easy foreign hydrocarbon migration, high brittle mineral content, and easy fracture production. This shale type is the most favorable shale oil exploration target in P<sub>1</sub>f within the Mahu Sag. In addition, this study reveals the relationship between rock lithofacies and shale oil potential, which provides a new idea for the potential evaluation of similar lacustrine shale oil.

## 1. Introduction

Shale oil is a type of self-generated and self-stored unconventional oil (including gas) originating from shale formations (fine-grained sedimentary rocks) as source rocks (Jarvie, 2012). Compared to conventional oil and gas, limited to complex geological conditions and difficult to exploit, shale oil has attracted increasing attention in countries worldwide due to its economic recovery aspects and very high resource potential (Zou et al., 2013). The shale revolution in North America reconstructed the global energy pattern, and revealed a very high resource potential of shale oil (Jarvie et al., 2007; EIA, 2014; Liu et al.,

2017a). U.S. shale oil reservoirs mainly include marine shales, largely located in the Bakken zone of the Williston Basin, the Eagle Ford zone in the western Gulf basin, the Sprague–Dawley zone, and the Anadarko Basin in the Woodford zone (Curtis et al., 2012; Chalmers et al., 2012; Jarvie, 2012). In contrast to U.S. marine shale formations, Chinese shale oil mainly occurs in continental shale formations, such as the Jimsar Lucaogou Formation, the Yanchang Formation in the Ordos Basin, the Shahejie Formation in the Dongying Sag of the Bohai Bay Basin, and the Qingshankou Formation in the Gulong, the northern Songliao Basin (Hu et al., 2018; Liu et al., 2019a, 2019b; Chen et al., 2020, 2021). Because of the limited development scale of lacustrine basins and complex

\* Corresponding author. State Key Laboratory of Petroleum Resources and Prospecting, China University of Petroleum, Beijing, 102249, China.

E-mail address: [jfjhtb@163.com](mailto:jfjhtb@163.com) (F. Jiang).

<https://doi.org/10.1016/j.geoen.2023.211501>

Received 12 June 2022; Received in revised form 28 December 2022; Accepted 28 January 2023

Available online 7 February 2023

2949-8910/© 2023 Elsevier B.V. All rights reserved.

depositional environment, lacustrine shale is very different from marine shale. Therefore, the previously proposed enrichment theory of marine shale oil cannot be applied to Chinese lacustrine shale oil.

Previous studies have indicated that lacustrine shale oil resources exhibit great potential, but their complex lithology complicates the evaluation of the shale oil potential (Liu et al., 2019a; Zeng et al., 2021). Shale oil resources do not always comprise mudstone but a range of fine-grained sedimentary rock (Jiang et al., 2013). Chao et al. (2017) noted that the heterogeneity of lithofacies is a key factor controlling the oil potential of deep shale. Different lithofacies vary in terms of hydrocarbon generation and storage and provide varying shale oil potentials (Wang, 2012; Nie et al., 2016; Chen et al., 2020). Moreover, the shale oil potential is closely related to the depositional environment. Compared

to freshwater basin shale, saline lacustrine shale has an earlier hydrocarbon generation time and higher oil and gas conversion efficiency (Yu et al., 2018a,b; Wang et al., 2020a; Cao et al., 2020). Therefore, it is of prospective significance to study the controlling effect of different rock types on the relative shale oil potential in complex depositional environments.

In 2017, the PetroChina Xinjiang Oilfield Company discovered the 1-billion-ton Mahu conglomerate oilfield, which is the largest conglomerate oilfield discovered worldwide (Zhi et al., 2021). The Fengcheng Formation ( $P_1f$ ) is not only the main source rock series in the Mahu oil area but also an important replacement area for current continental shale oil exploration in China (Yu et al., 2018a). Xinjiang Oilfield Company has deployed FC1, AK1, MY1 and MY2 wells to explore the

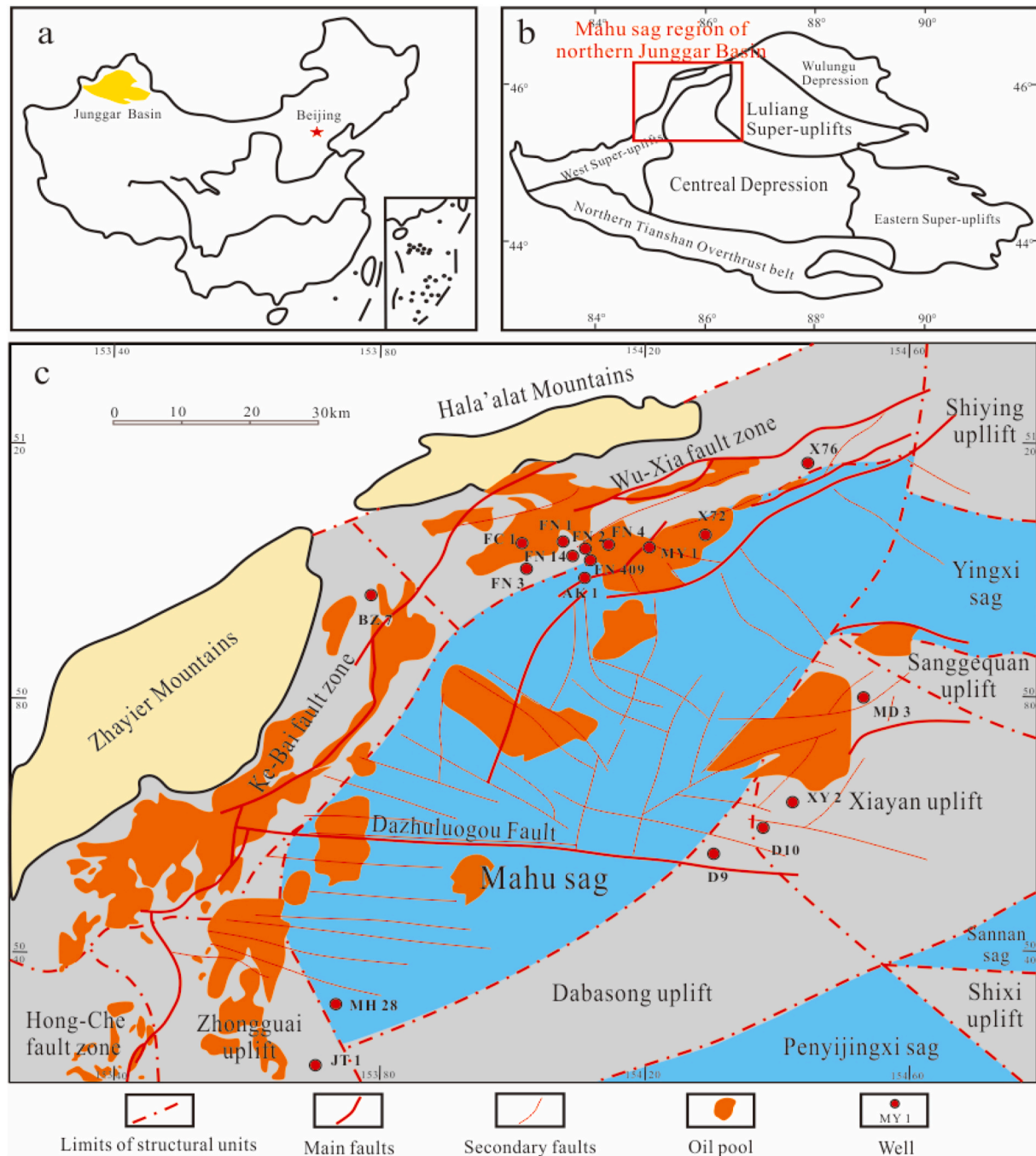


**Fig. 1.** (a) Geographical location of the Junggar Basin; (b) The main structural units of the Junggar Basin; (c) Structural units and well locations in Mahu Sag (modified from Feng et al., 2020).

shale oil potential of the P<sub>1</sub>f in the Mahu Sag. The MY1 well achieved a daily oil production rate of 23.06 t with a 2.5 mm nozzle in the 4579.00 m–4852.00 m section in 2020, and the MY1 well opened up a new milestone for shale oil exploration in the P<sub>1</sub>f. As of 2022, the MY1H and MY2 wells have made successive shale oil breakthroughs. P<sub>1</sub>f is the oldest high-quality alkaline lacustrine source rock developed thus far (Cao et al., 2020). This formation exhibits multistage high-efficiency hydrocarbon generation, a high hydrocarbon production rate and a notable shale oil potential. In contrast to other continental lacustrine

basin shales, this shale formation can provide a high applied research value (Tang et al., 2021). The shale oil in P<sub>1</sub>f within the Mahu Sag occurs at the early stage of exploration, and research on the shale oil potential and controlling factors is lacking. This paper aimed to study the differences in hydrocarbon generation, storage and migration among different lithofacies in this ancient alkaline lacustrine basin and further reveal the controlling effect of complex lithofacies on the shale oil potential.

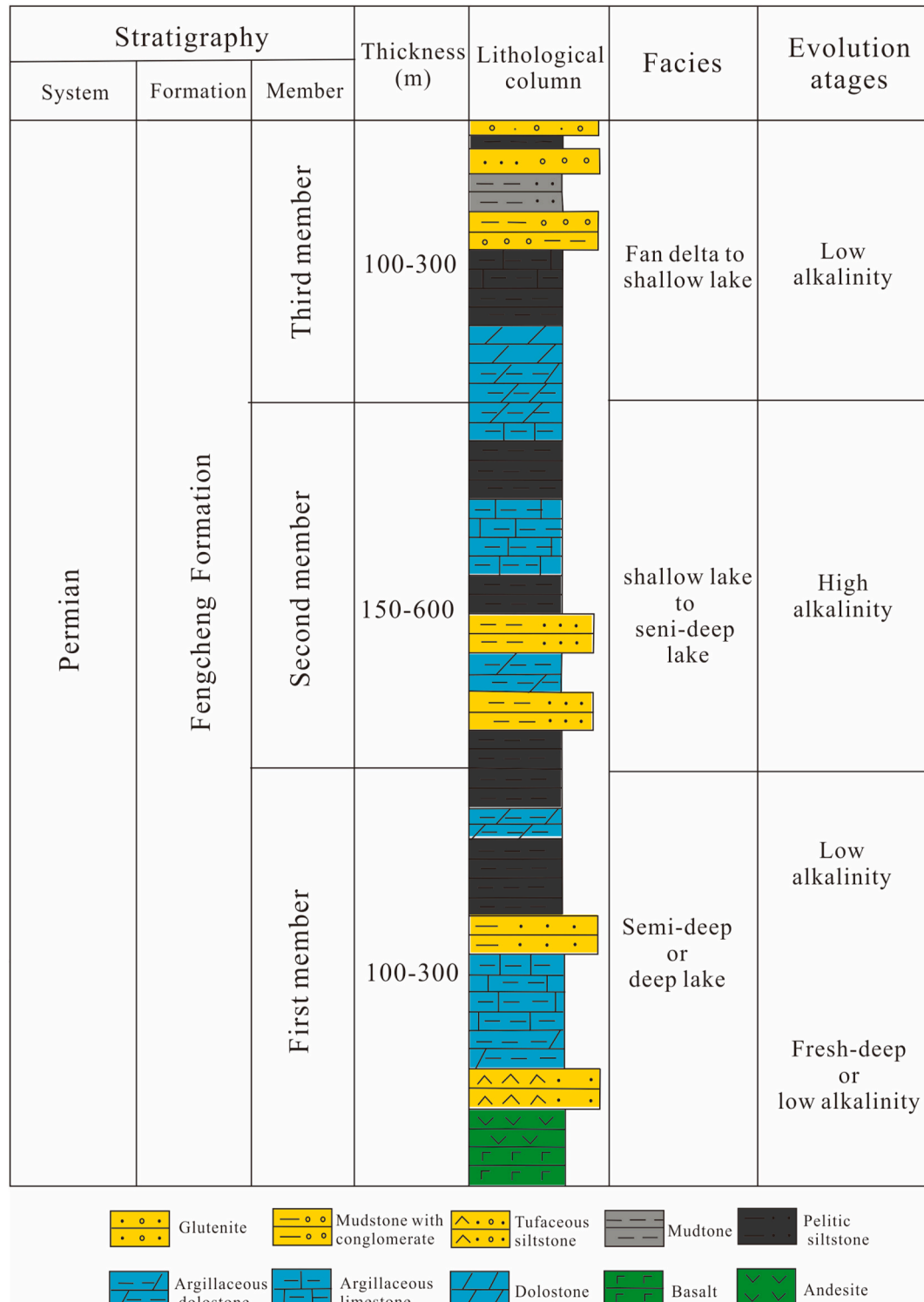


**Fig. 2.** Stratigraphic column of P<sub>1</sub>f (modified from Li et al., 2021).

## 2. Geological setting

The Junggar Basin is located in northwestern China (Fig. 1a), with 6 first-level structural units developed (Fig. 1b) (Wang et al., 2020a, ). The Mahu Sag is the northernmost secondary tectonic unit in the Central Depression. This Permian–Triassic sag exhibits the characteristics of a foreland basin; the Mahu Sag is a western uplift structure, with relatively well-developed faults after the Jurassic, and all of these faults are oriented along the northeast–southwest direction (Fig. 1c) (Li et al., 2016b; He et al., 2018).

The Mahu Sag is the most organic-rich hydrocarbon-generating sag in the Junggar Basin. P<sub>1</sub>f is the most important hydrocarbon-generating stratum and also a shale oil research hot spot today (Tang et al., 2021). In addition, P<sub>1</sub>f contains a set of alkaline lacustrine sedimentary systems, the burial depth is generally greater than 4000 m, and the burial depth of the depression center exceeds 5000 m. The sedimentary water salinity and rock type differ between the various layers of P<sub>1</sub>f (Zhang et al., 2018), and this formation can be divided into the 1st member of the Fengcheng Formation (P<sub>1</sub>f<sub>1</sub>), 2nd member of the Fengcheng Formation (P<sub>1</sub>f<sub>2</sub>) and 3rd member of the Fengcheng Formation (P<sub>1</sub>f<sub>3</sub>) from bottom to top. The bottom of P<sub>1</sub>f<sub>1</sub> mainly comprises tuff and mudstone, alkaline minerals are developed at the top, and frequent volcanic activities occurred during this period. During the P<sub>1</sub>f<sub>2</sub> period, the water body experienced the most intense evaporation and exhibited the highest salinity, mainly developing interbedded evaporite, saline mudstone and clastic rock layers, and the content of alkaline minerals was the highest. P<sub>1</sub>f<sub>3</sub> contains developed dolomitic rocks with fine-grained clastic rocks at the top (Fig. 2). Overall, the sources of the sedimentary materials in P<sub>1</sub>f are complex and diverse, and volcanic activity, terrigenous clastic materials, and salt minerals in the lacustrine basin yielded the complex fine-grained diamictite of P<sub>1</sub>f (Yu et al., 2019).

## 3. Samples and methods

### 3.1. Sample

Well MY1 is the shale oil exploration well in P<sub>1</sub>f. The Xinjiang Oil-field has produced 28 consecutive cores with a footage of 453.77 m and a core length of 444.7 m. The core obtained from the P<sub>1</sub>f is 365.38 m in length. Moreover, the oil immersion grade is 6.12 m, the oil spot grade is 175.03 m, and the oil stain grade is 184.23 m. The overall oil content is suitable, and the samples are representative. In this study, samples were taken from the focal well MY1 and the surrounding wells FN1, FN2, FN3, FN14, MH28, AK1 and FN409 (Fig. 1c).

### 3.2. Methods

Total organic carbon (TOC), rock pyrolysis and whole-rock analyses were performed of the 150 samples. First, the sample surface was cleaned, and a given sample was ground to 200 mesh. Second, 0.1 g powder was collected for pickling treatment, the remaining sample material was rinsed with 15% dilute hydrochloric acid for three days, an oven was used to dry the sample for 10 h, and finally, a CS-230HC analyzer was used for TOC determination. Rock pyrolysis analysis was conducted on a Rock-eval II. Through grinding, a 0.1-g 200-mesh sample was obtained, which was initially heated at a heating rate of 25 °C/min to 300 °C for 3 min. We determined the free hydrocarbon content (S<sub>1</sub>) and then measured the pyrolyzed hydrocarbon content (S<sub>2</sub>) as the temperature was increased to 600 °C, and the temperature corresponding to the highest peak of pyrolyzed hydrocarbons could be denoted as T<sub>max</sub>. Finally, a sample was first ground to 300 mesh with a grinder and subsequently manually ground with a mortar. Five grams of the thusly prepared sample was evenly spread on a glass slide. Then, the slide was placed in a ZJ207 Bruker D8 instrument for mineral composition analysis.

With the use of international standard ISO 17246:2010, the Ro was

determined according to the procedure of Xie et al. (2016). Micro-components were obtained following international standard ISO 7404:2009, and 11 samples were selected to determine microcomponents.

To qualitatively reveal the pore morphology and characteristics, the pore characteristics were analyzed under a Sigma-500 scanning electron microscopy (SEM) instrument. Samples were fabricated into a size of 10\*5\*1.5 mm (width, height and length), mounted in resin after polishing, and observed after gold plating. To reveal the pore structure characteristics, 12 samples were selected for mercury intrusion and nitrogen adsorption experiments. The mercury intrusion and nitrogen adsorption experiments were conducted with a Kantar PoreMaster-60 mercury injection instrument and an Autosorb iQ instrument, respectively. The maximum mercury injection pressure could reach 200.33 MPa, and pores with a minimum pore throat radius of 4 nm could be measured. For the N<sub>2</sub> adsorption experiments, the samples were ground to 80 mesh and dried under vacuum at 150 °C for 10 h. The experimental temperature was −196 °C, the pressure ranged from 973 to 127.0 MPa, and pores with a diameter of 0.35–200.6 nm could be identified. To further study the pore structure and connectivity, four petrographic samples were selected for micro-computed tomography (CT) scanning under a Zeiss laboratory micron high-resolution 3DX ray microscope. The experimental voltage was 120 kV, the resolution was 3.14 μm, and the scanned data volumes were processed in Avizo software.

The calculation method of  $\Delta S_1$  of free hydrocarbon index is shown in Li et al., (2016a, ). In this method, the regression equation is first obtained by measuring the vitrinite reflectance (R<sub>o</sub>) of the sample, through which the R<sub>o</sub> at any depth can be calculated. Then, the kerogen type of the sample is determined. For different types of kerogens, the HCGR of any depth sample is calculated according to the calculated hydrocarbon generation rate (HCGR) equation established by the kerogen generation experiment. For the corresponding hydrocarbon generation rates (HCGR) of different types of kerogens, the Biyang sag is a terrestrial salt lake sedimentary, which is similar to the sedimentary environment of the Mahu sag. In this study, the hydrocarbon expulsion and migration status of shale samples from the P<sub>1</sub>f were characterized by using the curve plates of different types of kerogen hydrocarbon generation in the Biyang sag. Finally, the hydrocarbon generation quantity (HCGQ) is calculated by  $HCGQ = HCGR * TOC$ , and the free hydrocarbon index  $\Delta S_1 = HCGQ - S_1$ .

## 4. Results

### 4.1. Mineralogy and lithofacies classification

#### 4.1.1. Mineralogy

Based on the mineralogy, the mineral composition of P<sub>1</sub>f is complex (Fig. 3), mainly comprising quartz and dolomite, followed by clay minerals, calcite, plagioclase, K-feldspar, and a small amount of pyrite, gypsum, alkaline minerals, etc. The minerals can be divided into three combinations, and it is found that the shale mineral composition indicates high carbonate and felsic mineral contents, with average contents of 45% and 36%, respectively, and low-clay mineral (average 8.9%) characteristics. In addition, quartz and dolomite account for more than 80% of the felsic and carbonate minerals, respectively. Overall, the mineral composition exhibits significant longitudinal changes, with carbonate and other minerals varying according to opposite trends (Fig. 4).

#### 4.1.2. Lithofacies classification

The lithofacies refers to the total of all lithological characteristics of sedimentary rocks in a specific environment, including mineral composition, color, grain size and distribution, and is crucial for the analysis of depositional processes and depositional environments (Loucks and Ruppel, 2007; Singh et al., 2009). Different lithofacies can exhibit notable differences in the oil and gas hydrocarbon generation



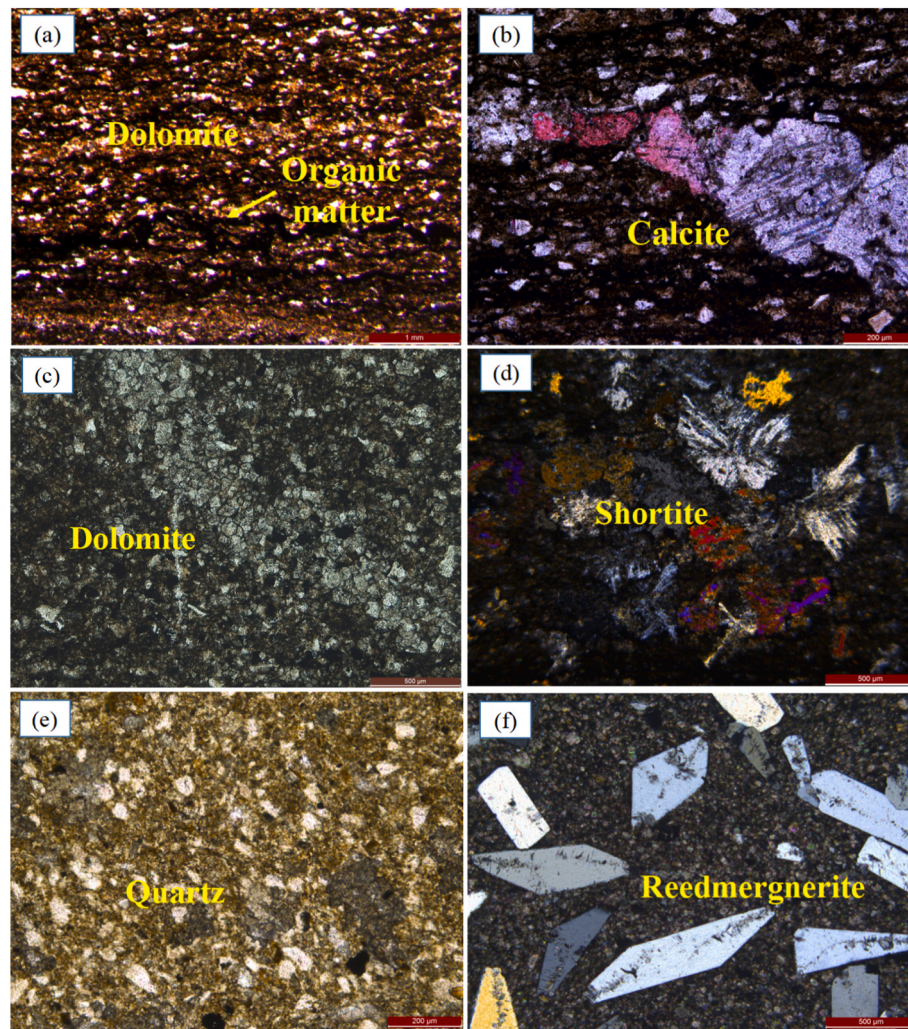


**Fig. 3.** Microscopic photo of petrology. (a) Lamellar bands of organic matter and dolomite, MY1, 4585.16 m; (b) Calcite, MY1, 4747.46 m; (c) Dolomite, MY1, 4750.85 m; (d) Shortite, MY1, 4750.85 m; (e) Quartz, FN3, 3955.58 m; (f) Reedmergnerite, FN3, 4147.50 m.

potential and storage capacity, thus yielding varying shale oil and gas potentials (Zou et al., 2013). Lithofacies have been classified by predecessors (Loucks and Ruppel, 2007; Chen et al., 2016; Liu et al., 2017b; Peng et al., 2019; Liu et al., 2018; Wang et al., 2020b), but no unified standard has been formed.

Based on the classification of the three main minerals (felsic, carbonate and clay minerals), a tertiary diagram was established for lithofacies identification (Fig. 5). Shale can be divided into felsic, mixed, carbonate and clayey shale types. Carbonate shale can be further divided into lime and dolomitic shale types. The X-ray diffraction (XRD) results indicate that four types of lithofacies can be identified in regard to P<sub>1</sub>f, namely, felsic, mixed, dolomitic and lime shale types.

## 4.2. Organic geochemical characteristics

### 4.2.1. Organic matter abundance and generation potential

A sufficient amount of organic matter in source rocks constitutes the material basis for the formation of oil and gas and is the main factor determining the hydrocarbon generation potential. The TOC content in P<sub>1</sub>f ranged from 0.08% to 2.95% (average: 0.78%), the S<sub>1</sub> content ranges from 0.06 to 8.39 mg/g (average: 1.26 mg/g) and the S<sub>2</sub> content ranging from 0.03 to 19.9 mg/g (average: 2.42 mg/g). Therefore, free hydrocarbons (S<sub>1</sub>) and cracked hydrocarbons (S<sub>2</sub>) constitute the hydrocarbon generation potential (PG), and the PG value ranged from 0.12 to 20.81 mg/g (average: 3.67 mg/g). In this study, PG and TOC present a positive

correlation (Fig. 6a), and the distribution of TOC and PG indicates that the shale of P<sub>1</sub>f has a good OM abundance (Fig. 6e and f). Among 150 samples, the proportion of TOC reaching medium-good source rock is up to 67%, among which the proportion of good-excellent source rocks is up to 25%, and the proportion of PG reaching fair-good source rock is up to 65.3%. All these data indicate that most core samples of P<sub>1</sub>f shale are fair-good source rocks. In addition, the relationships between S<sub>2</sub> and TOC, and HI and TOC can all reflect the hydrocarbon generation potential of oil shale (Zhang et al., 2020; Zou et al., 2018; Peters and Cassa, 1994; McCarthy et al., 2011). It also shows that the source rocks in the P<sub>1</sub>f are mainly fair-good source rocks and have certain hydrocarbon generation potential on the whole.

The hydrocarbon generation potential of the different lithofacies shale varied (Table 1). The dolomitic and lime shale attained the large TOC value, and the felsic and mixed shale types exhibited similar TOC average values. The P<sub>1</sub>f shale total TOC content is low, which can be attributed to the presence of more terrigenous clastic elements, which can dilute organic matter (Mohialdeen and Hakimi, 2016; Hakimi et al., 2016). Regarding the HI index, dolomitic shale attained the highest value. The average value of the HI index was 302.79 mg/g, and the maximum value could reach more than 673.90 mg/g. The HI index value of mixed shale was the lowest (average: 221.43 mg/g), and the distribution range was similar between the felsic and lime shale types. However, the currently analyzed HI index is the residual hydrocarbon generation potential, and the original hydrocarbon generation potential



Fig. 4. Mineral composition characteristics of Well MY1.

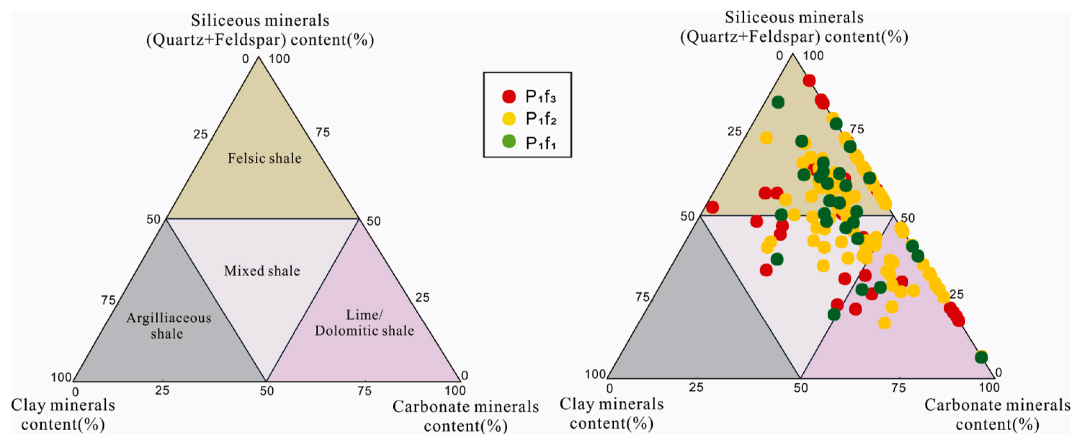


Fig. 5. Lithofacies identification triangle of P<sub>1</sub>f.

can be higher. The relationship between  $S_2$  and TOC can be used to evaluate the original hydrocarbon generation potential ( $HI_0$ ) of the different lithofacies. The slope of the regression curve represents the trend of the original hydrocarbon generation potential (Fig. 6d). The results indicated that the original hydrocarbon generation potential ( $HI_0$ ) of the dolomitic, felsic, mixed and lime shale types reached 601.63, 360.44, 367.55 and 288.63 mg/g, respectively. Overall, the dolomitic and felsic shale types attained a high hydrocarbon generation potential, while the calcareous and mixed shale types attained a low hydrocarbon generation potential.

#### 4.2.2. Organic matter type

When determining the ability of source rocks to generate hydrocarbons, the kind and source of organic matter are of paramount importance. The OI vs. HI map was used to classify the kerogen type (Tissot and Welte, 1984; Peters and Cassa, 1994), and the results demonstrated that the P<sub>1</sub>f shale was mainly II kerogen type, of which the type I kerogen was largely observed in the felsic and dolomitic shale types, while mixed

shale mainly included the type II<sub>2</sub> and III kerogen types (Fig. 7a). In addition, TOC and  $S_2$  maps can be used to determine the kerogen type (Langford and Blanc-Valleron, 1990; Chen and Jiang, 2018), and the results indicated that almost all samples occurred within the range of type II<sub>2</sub> and II<sub>1</sub> kerogens (Fig. 6d). Since the results of rock pyrolysis analysis are susceptible to contamination, microscopic observation was used to determine the content of different microscopic components in kerogen, and the kerogen type could be more reliably determined (Hutton, 1994; Scott, 2002). The microscopic composition of the P<sub>1</sub>f shale was dominated by exinite (average: 72%) and sapropelinite (average: 31%), with a small amount of vitrinite and inertinite. The index of organic matter TI might be utilized to better differentiate between the different kinds of biological materials (Tao et al., 2012; Chen et al., 2021), mainly type II<sub>2</sub> kerogen (Fig. 7b), and the microscopic composition is consistent with the rock pyrolysis analysis results.

#### 4.2.3. Thermal maturity

Vitrinite reflectance ( $R_o$ ) and pyrolytic  $T_{max}$  are the most commonly

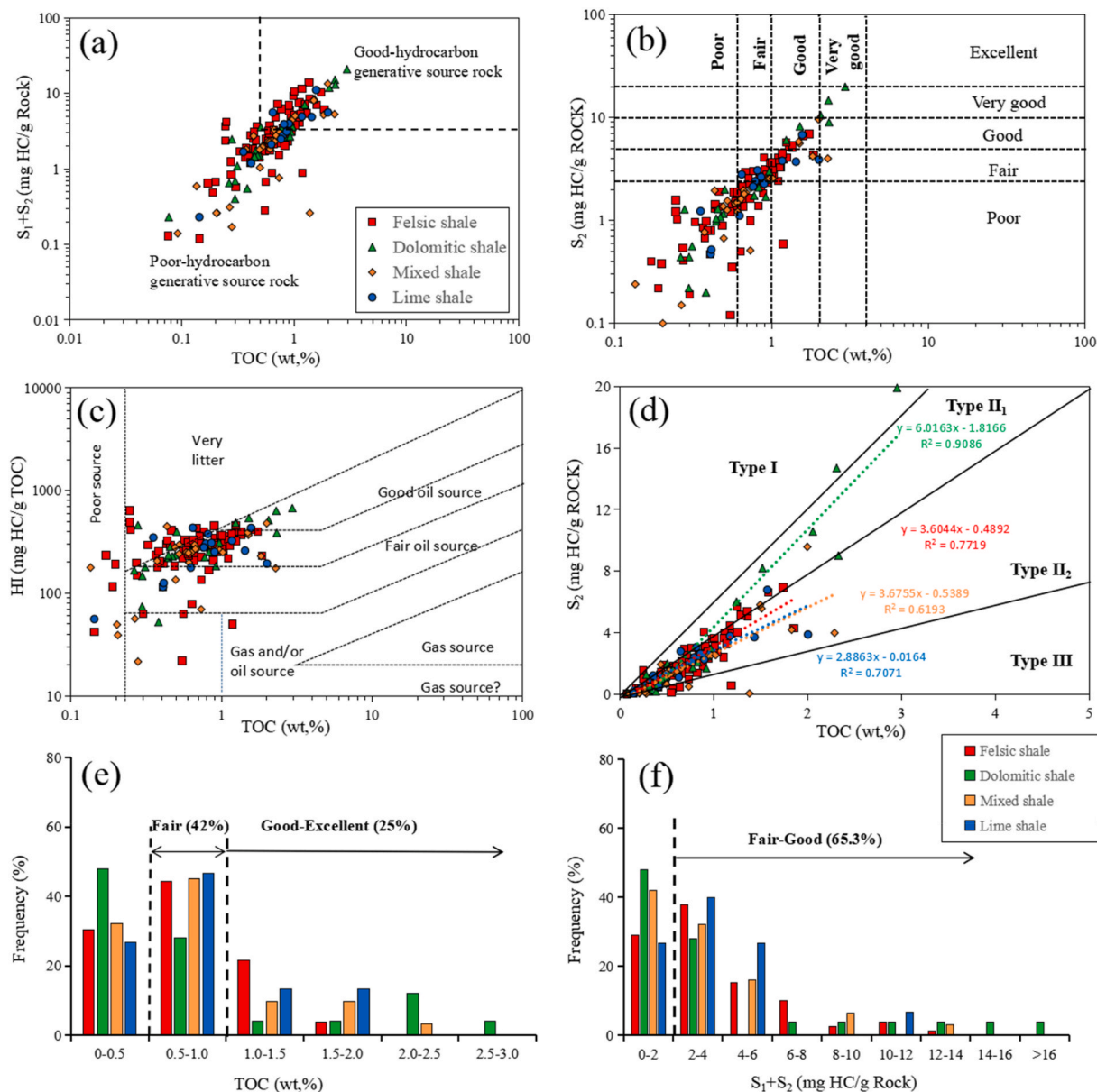


**Fig. 6.** (a) Pyrolysis hydrocarbon generation potential  $S_1+S_2$  and TOC to evaluate source rock quality (b) Pyrolysis  $S_2$  and TOC to evaluate source rock quality (c) Hydrogen index HI and TOC to evaluate source rock quality (d) Pyrolysis of  $S_2$  and TOC to classify organic matter types and evaluate the hydrocarbon generation potential of rocks (e) Frequency distribution diagram of TOC (f) Frequency distribution diagram of potential hydrocarbon generation  $S_1+S_2$ .

**Table 1**  
TOC and Rock-Eval parameters for P<sub>1</sub>f.

lithofacies	TOC	S <sub>1</sub>	S <sub>2</sub>	PG	HI	OSI
	wt. %	mg HC/g Rock	mg HC/g Rock	mg HC/g Rock	mg HC/g TOC	mg HC/g TOC
Felsic shale	0.08–1.85	0.06–8.39	0.03–6.94	0.12–13.79	22.00–640.55	15.15–1267.55
	0.74	1.54	2.16	3.70	274.88	214.73
Dolomitic shale	0.08–2.95	0.11–4.03	0.12–19.9	0.23–20.81	52.33–673.90	30.82–423.39
	0.89	0.77	3.12	3.89	302.75	128.03
Mixed shale	0.09–2.29	0.09–3.78	0.05–12.43	0.14–13.36	5.07–479.95	13.78–278.30
	0.78	0.99	1.99	2.97	221.43	122.44
Lime shale	0.14–2.00	0.15–4.26	0.08–6.79	0.23–11.05	55.94–434.10	41.86–431.01
	0.86	1.18	2.46	3.64	266.17	141.89

Note: 0.08–2.31, 0.77 stands for Min.-Max., Ave.; OSI =  $S_1/TOC \times 100$ ; HI =  $S_2/TOC \times 100$ ; PG =  $S_1+S_2$ .

used indicators to determine thermal maturity. The pyrolysis  $T_{max}$  index can be obtained quickly and at a low price, but it is easily affected by asphaltene, kerogen type, and mineral composition (Kruge, 1983; Peters

et al., 2018; Katz and Lin, 2021). Therefore, the vitrinite reflectance ( $R_o$ ) is regarded as the best discriminant index. According to the results of the vitrose reflectance ( $R_o$ ) experiment of 42 samples in this study, the



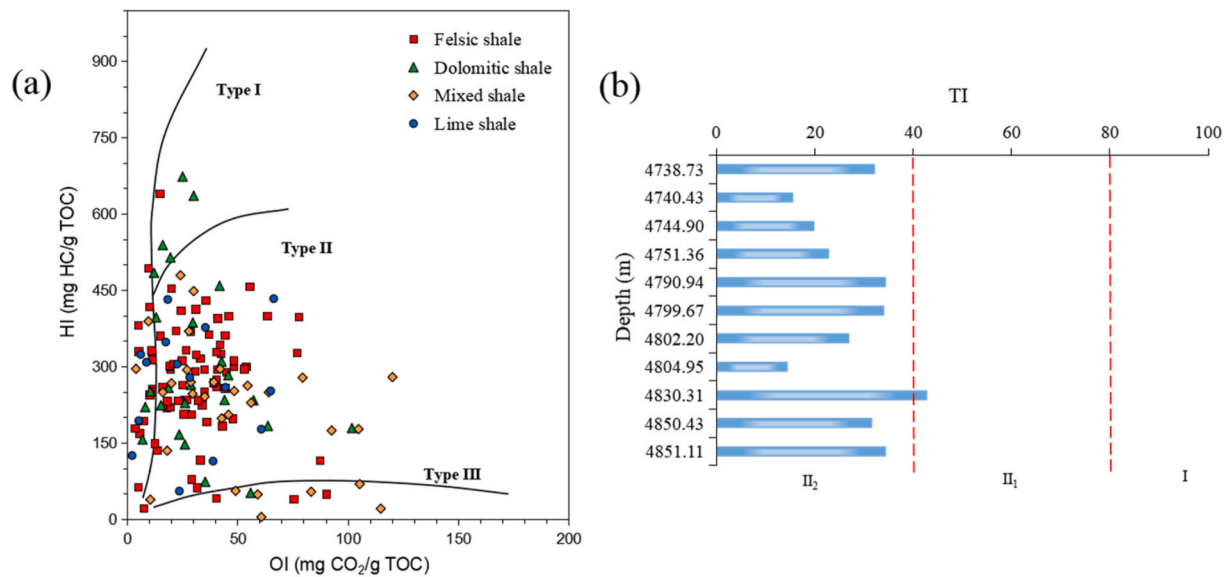


Fig. 7. Classification of organic matter types (a) Diagram of OI vs. HI. (b) Organic matter type index (TI) diagram of microcomponents in Well MY1.

vitroinite reflectance ( $R_o$ ) increased with the increase of depth, which had a good correlation, and revealed that the source rocks of the P<sub>1</sub>f had reached the mature-high maturity stage (Fig. 8). Combined with previous studies (Yu et al., 2018a; Feng et al., 2020; Li et al., 2021; Tang et al., 2021), it is suggested that the P<sub>1</sub>f shale is at the peak of oil generation at the present stage, reaching the mature-high maturity stage.

#### 4.3. Reservoir space characteristics

##### 4.3.1. Pore types and fractures

Fractures represent the most important pore type in shale oil

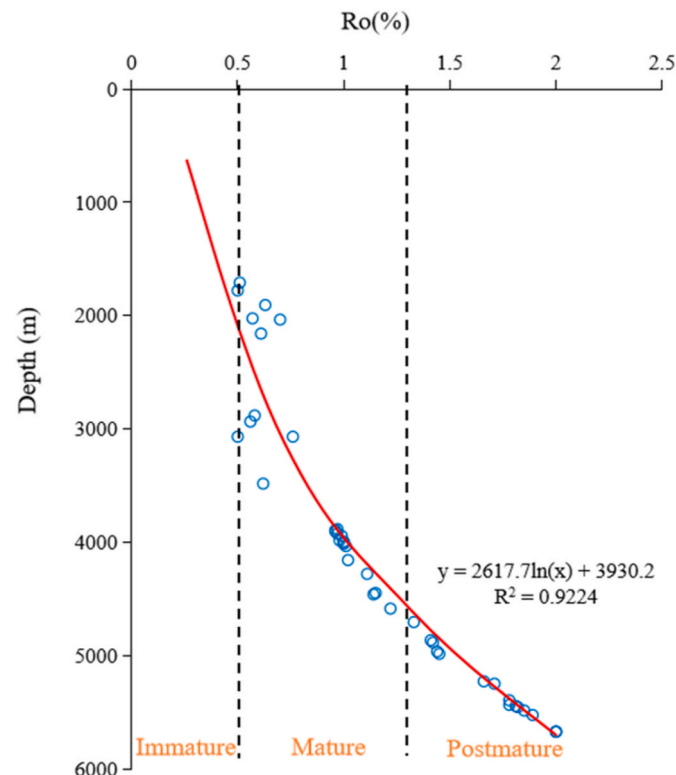


Fig. 8. Ro (%) vs depth plot showing the maturity of the P<sub>1</sub>f.

research and can significantly improve shale storage and migration performance levels. Fractures in the shales of the P<sub>1</sub>f are mainly bedding fractures and structural fractures (Fig. 9). Bedding fractures with a long extension and small micron-scale width could be observed in laminar or well-bedded shale intervals, and these fractures were widely developed and discontinuous laterally. The density of the fractures observed in cores is about (4–6) fractures/10 cm, a width usually less than 2 mm. Fluorescence scanning of the core indicated notable fluorescence, which represents hydrocarbon migration within the shale. Bedding fractures were developed in all lithofacies, but it should be noted that high-angle structural fractures were observed in felsic shale. High-angle fractures are generally perpendicular to the layer or intersect at a high angle and are characterized by longitudinal penetration of the layer. Fractures were observed in cores ranging in width from 2 to 3 mm and up to 10–15 cm in length. As a good migration pathway, these high-angle fractures were usually filled with bitumen and occurred in communication with different thin layers, representing important channels connecting hydrocarbon-rich and hydrocarbon-depleted layers.

A large number of nano- and microscale pores could be observed under the SEM instrument, and these pores could be divided into interparticle, intraparticle and organic pores and microcracks. Mineral-related inorganic pores were the most common pore type in the P<sub>1</sub>f samples, and these pores were widely distributed and relatively large, up to 5  $\mu$ m in diameter. Organic pores were relatively undeveloped and only found in very few samples, but the development of organic pores could significantly increase the storage space. Microfractures were developed in all lithofacies, but the pore types and shapes of the different lithofacies varied.

Microfractures and intergranular pores were the most common in felsic shale. Pores mainly comprised micron-scale intergranular pores between quartz and carbonate mineral particles, most of which included slit-type or triangular pores, and the average pore size ranged from several hundred nanometers to several micrometers (Fig. 10a and b). Microfractures were widely distributed in felsic shale, forming an effective fracture network for hydrocarbon storage (Fig. 10c). Partially compacted feldspar intragranular dissolution pores could also be observed (Fig. 10f), but organic pores were less developed in felsic shale, and these pores were elliptical, isolated, and exhibited a poor connectivity (Fig. 10g).

Various pore types were developed in dolomitic shale, and the most abundant pores were intragranular pores, among which dissolution pores affected by organic hydrocarbon generation were developed in



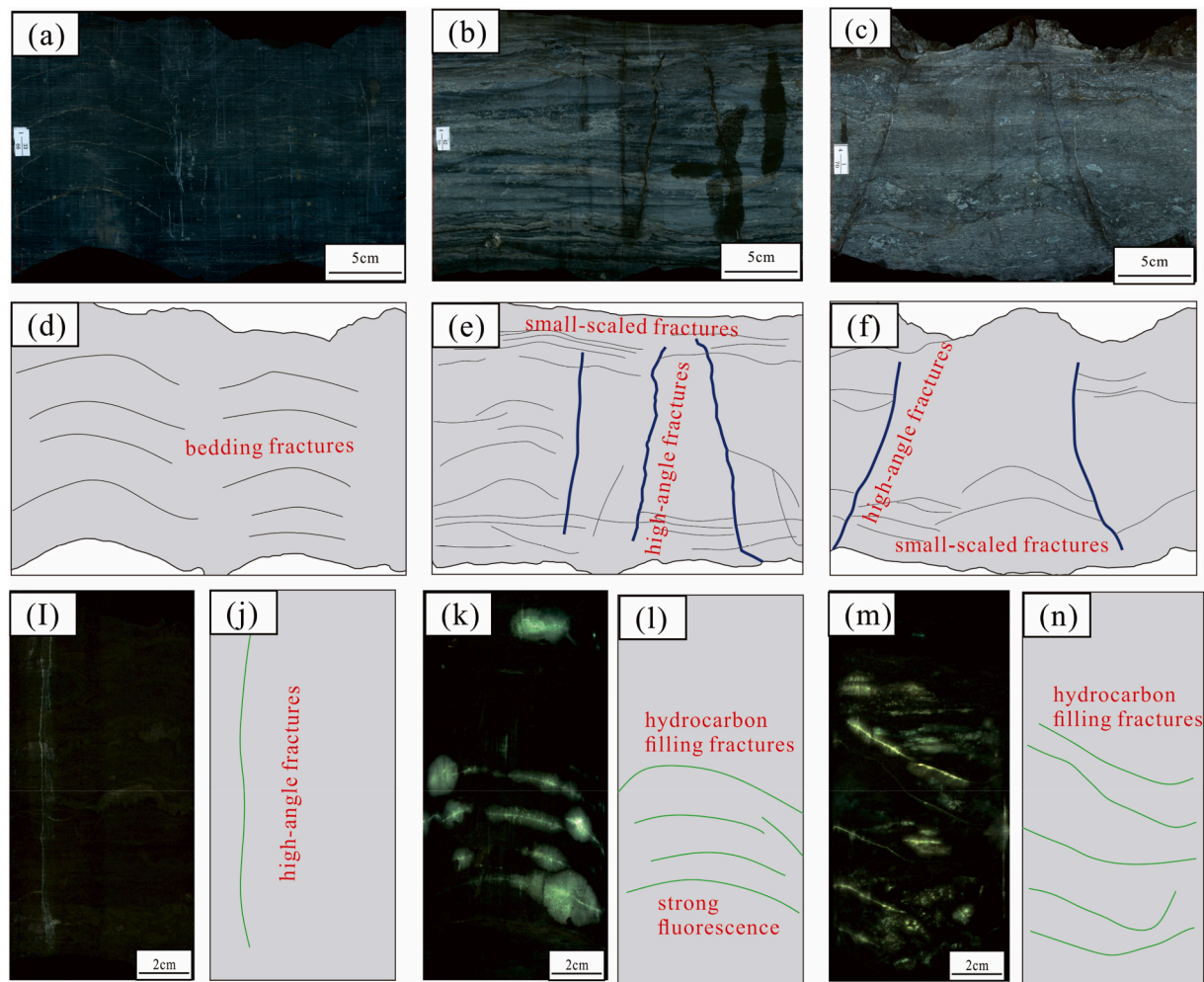


Fig. 9. Fracture characteristics of shale in P<sub>1</sub>f.

dolomite and calcite minerals (Jarvie et al., 2007). The dissolution pores were wedge-shaped or polygonal pores, with a diameter of several micrometers, but the connectivity was low (Fig. 10d and e). There occurred few intergranular pores and microfractures, and the pore size was small. The development of pores in lime shale was similar to that in dolomitic shale, but the pore size was larger than that in dolomitic shale, and a small number of organic pores can be observed.

In mixed shale, intra- and intergranular pores were developed, and a small amount of microfractures could be found. The intercrystalline pores in clay minerals appeared as flakes or layers mainly due to compaction (Fig. 10h and i), and owing to clay mineral adsorption and expansion, the pore size was small (<100 nm), and the connectivity was low. Compared to the previous three lithofacies, the pore characteristics of mixed shale are not conducive to oil and gas accumulation.

#### 4.3.2. Pore size distribution

**4.3.2.1. MICP.** The pore size distribution in the different lithofacies was obtained in a high-pressure mercury intrusion experiment (Fig. 11). The pore size distribution characteristics of the different lithofacies were generally similar, exhibiting similar multimodal characteristics in the 3–200 nm and 10–100  $\mu\text{m}$  ranges. It should be noted that the pore size distribution in the four lithofacies revealed obvious peaks in the 10–100  $\mu\text{m}$  range, and felsic shale attained the highest peak within this range. Combined with the SEM observation results, microscale macropores mainly included microfractures and large dissolution pores, and microfractures were observed in all four lithofacies types. Therefore, it

could be considered that the pores in the 10–100  $\mu\text{m}$  range largely included microcracks and larger dissolution pores. The pore size distribution curves demonstrated obvious peaks in the 3–200 nm range, but the four lithofacies exhibited different characteristics. Based on the sequence of felsic shale-dolomitic shale-lime shale-mixed shale, the pore size peak position shifted to the left, and the peak decreased, indicating a significant decrease in pore radius and pore number.

**4.3.2.2.  $N_2$  adsorption.** Low-temperature nitrogen adsorption-desorption curves for the different lithofacies shale are shown in Fig. 12. With increasing relative pressure, the adsorption isotherm curves for each lithofacies all belong to the type IV isotherm of the reverse S type (Sing et al., 1985). At a lower pressure ( $P/P_0 < 0.5$ ), monolayer adsorption transitioned into multilayer adsorption. For  $P/P_0$  close to 1, the adsorption curve did not reach saturation adsorption (macropore filling). An obvious hysteresis loop (corresponding to capillary condensation in mesopores) emerged in the isotherm adsorption curve at approximately  $P/P_0 = 0.5$ , and the shape of the hysteresis loop could be used to infer the shale pore geometry (Tian et al., 2013; Liu et al., 2019b; Li et al., 2019a). Among the various lithofacies, the hysteresis loop morphology of felsic and lime shale indicated the H2 and H3 composite type, the pores were mainly ink bottle-shaped pores, and some pores included omnidirectional parallel-plate-shaped slit pores. This composite pore space is conducive to the storage and transport of oil and gas. The hysteresis loops of dolomitic and mixed shale indicated the H3 type, the hysteresis loops were narrow, and the adsorption and desorption curves almost coincided, reflecting the presence of

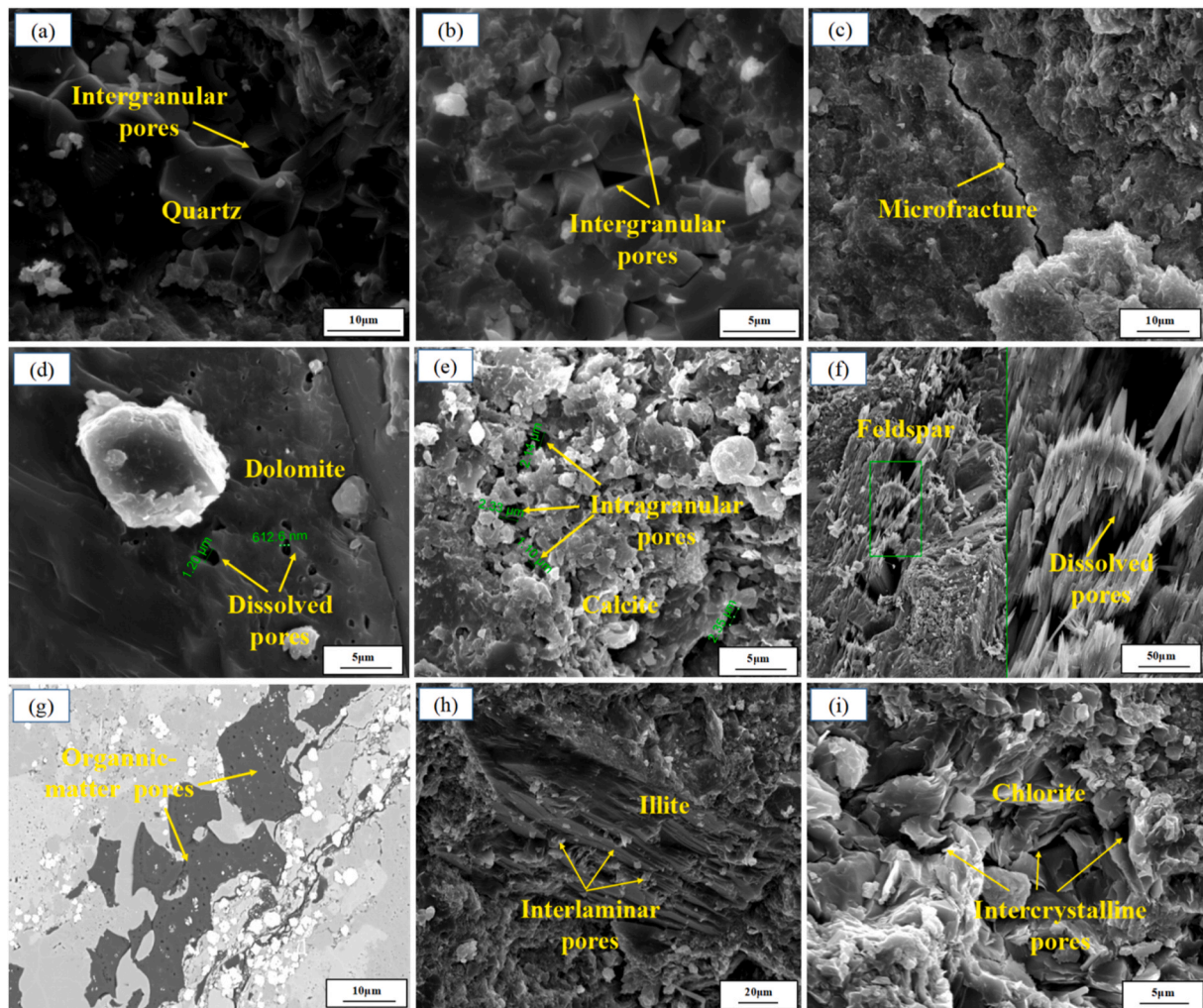


**Fig. 10.** SEM photo of P<sub>1</sub>f (a) Quartz intergranular pores, AK1, 5667.8 m (b) Carbonate mineral intergranular pores, MY1, 4742.16 m (c) Microfractures, AK1, 5667.8 m (d) Dolomite Dissolution pores, MH28, 4931.30 m (e) Calcite inner pores, FN409, 4526.35 m (f) Feldspar dissolution pores, FN3, 4147.50 m (g) Organic pores, MY1, 4710.99 m (h) Illite interlayer pores, AK1, 5667.8 m (i) Chlorite intercrystalline pores, AK1, 5667.8 m.

parallel-plate-like slit pores in the samples. The pores could be classified according to the IUPAC as micropores (<2 nm), mesopores (2–50 nm), and macropores (>50 nm). Fig. 13 shows that the pores in felsic and dolomitic shale largely included meso- and macropores, macropores were more developed than were micropores, and the pore structure was suitable. The proportion of micro-, meso- and macropores in lime shale was similar, and the pore structure was general. Mixed shale was dominated by micro- and mesopores, with the worst pore structure.

#### 4.3.3. Reservoir space distribution and connectivity

The structure of the shale storage space is complex, not isolated in regard to the distribution but interconnected in space, forming a complex pore network system. A 3D pore model, pore connectivity model and pore ball-and-stick model can be established via 3D reconstruction under micro-CT scanning, and the internal structure of shale reservoirs can then be effectively characterized.

The micro-CT scanning results indicated (Fig. 14) that the spatial structure of the shale oil reservoirs in P<sub>1</sub>f was mainly controlled by the lithofacies, and the pore development and connectivity in the different lithofacies varied (Table 2). The CT-derived porosity of felsic shale was 7.5%, that of lime and dolomitic shale was 5.7% and 4.6%, respectively, and that of mixed shale was the lowest, at only 2.1%. Felsic shale contained the largest number of pores and throats. The pore model revealed that the pores were clustered and uniformly distributed. The pore radius

could reach up to 50 µm, and the average pore radius was 9.88 µm, which yielded the largest pore coordination number. Compared to the other lithofacies, felsic shale contained densely developed pores, larger pore sizes, and optimal throat connectivity (the most connected throats), and a suitable three-dimensional pore network was readily formed. Lime and dolomitic shale exhibited similar pore development levels and were controlled by laminae. Pores were developed along laminae and were distributed in sheets, with relatively small pore sizes (an average pore size of 9 µm). The pore ball-and-stick model indicated that the throat distribution was uneven and exhibited flake-like features. Compared to dolomitic shale, the pore and throat diameters in lime shale were larger. Mixed shale pores were isolated but well developed, with the smallest number of pores and throats, and the throats were scattered and poorly connected.

#### 4.4. Hydrocarbon migration

In the shale oil system, there exists both primary migration within the source rock and short-range secondary migration into adjacent units (Li et al., 2016a; Han et al., 2019; Chen et al., 2020; Zou et al., 2019). Li et al. (2016a) proposed a new index of free hydrocarbons,  $\Delta S_1$ , to characterize the state of shale hydrocarbon expulsion and migration and to predict hydrocarbon migration from a given shale unit to an adjacent unit.

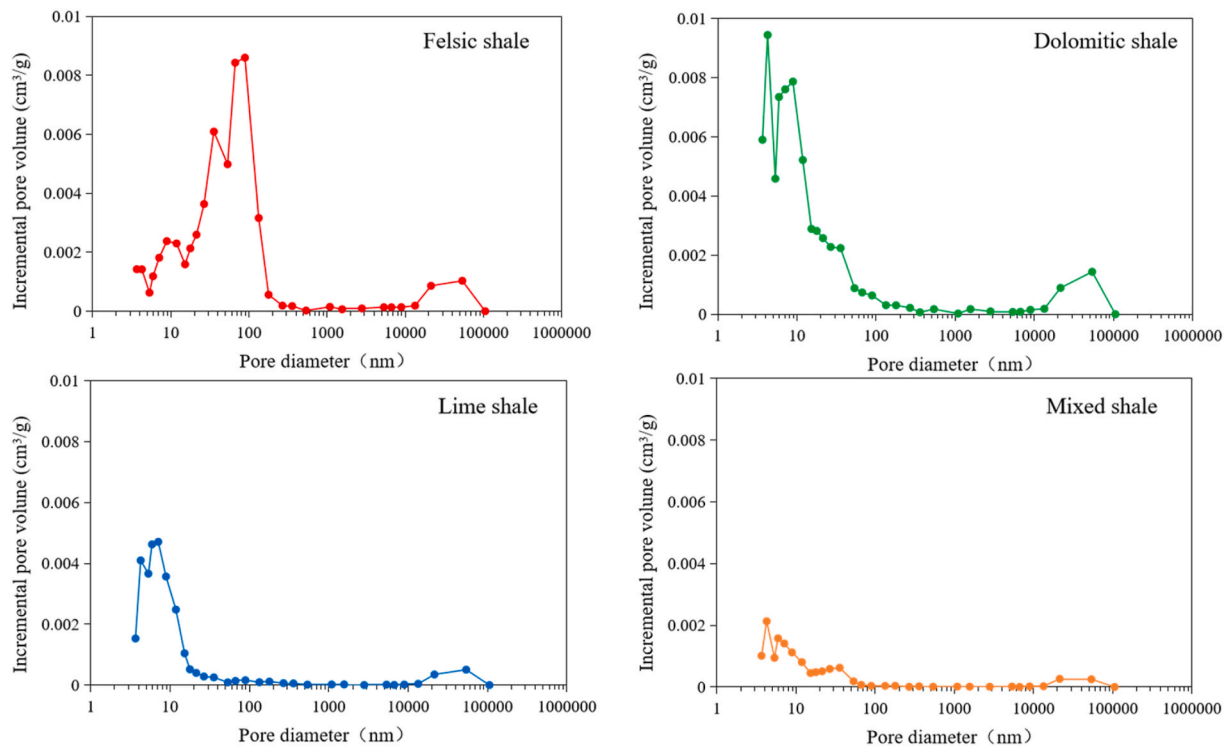


Fig. 11. Distribution of pore volume versus pore size for different lithofacies.

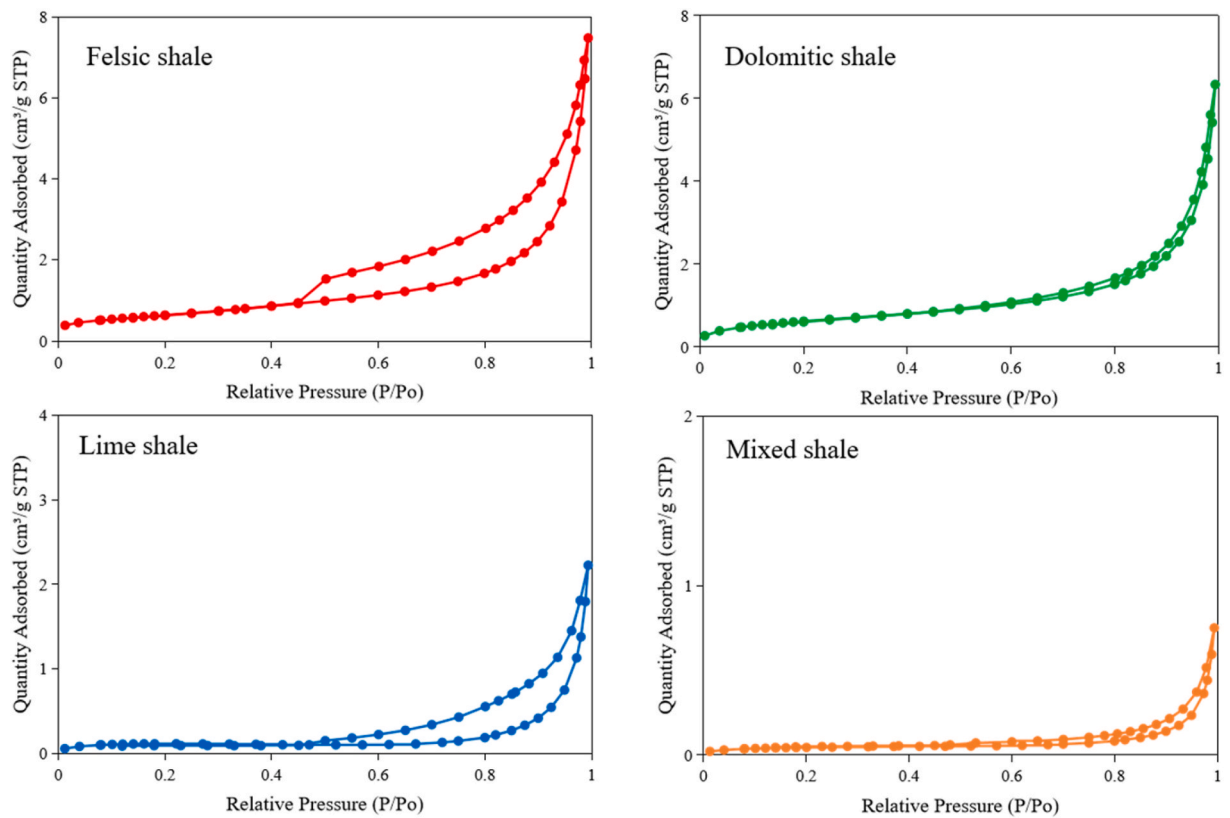


Fig. 12.  $N_2$  adsorption-desorption curves of different lithofacies.

The free hydrocarbon index  $\Delta S_1$  data of some samples are shown in Table 3. The results indicated that the free hydrocarbon index  $\Delta S_1$  could be divided into three types (Table 4). Type I mainly included

dolomitic shale and a small number of felsic shale samples (Fig. 15). In addition, the  $\Delta S_1$  value of the M-99 and M-103 dolomitic shale samples could reach  $-7$  mg HC/g rock, indicating that dolomitic shale exhibits a



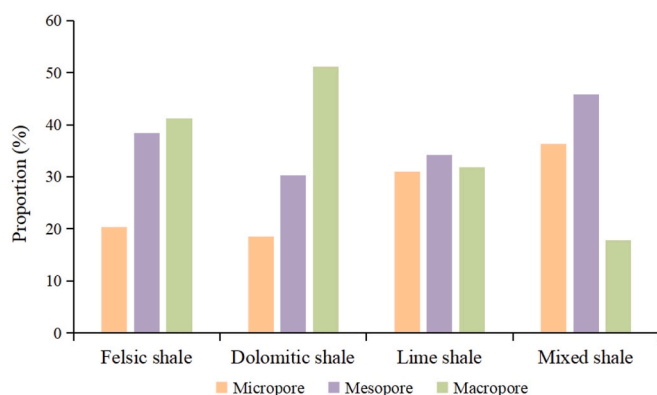


Fig. 13. The proportion of micro, meso and macro pores in different lithofacies.

notable ability to expel hydrocarbons. The four shale lithofacies all included type II, and the  $\Delta S_1$  value of these samples approached 0, indicating that there is no hydrocarbon migration phenomenon in the shale system self-generation and self-accumulation process. Type III almost entirely comprised felsic shale, with a small number of lime shale samples. In addition, the  $\Delta S_1$  value of the M-67, M-70, and M-71 felsic shale samples could reach 6 mg HC/g rock, and the free hydrocarbon index  $\Delta S_1$  values of the other samples also included high positive values. This suggests that there occurred a large amount of foreign hydrocarbon migration in the felsic shale system, and the ability to receive hydrocarbons was notable. Most of the lime shale samples were similar to the mixed shale samples, indicating a closed unit. However, some samples received a small amount of foreign hydrocarbons, but the ability to receive hydrocarbons was low.

## 5. Discussion

### 5.1. Shale oil potential

The resource potential of shale oil can generally be evaluated by the rock oil content. Scholars in China and abroad have usually evaluated the shale oil content based on pyrolysis parameter  $S_1$  and chloroform bitumen A. Pyrolysis parameter  $S_1$  refers to both the free and volatile hydrocarbons measured in pyrolysis experiments at 300 °C, chloroform bitumen A is the extractable organic matter in a given sample. (Barker, 1974; Espitalié et al., 1977; Tissot and Welte, 1984).  $S_1$  cannot represent the presence of the heavy component of oil, whereas Chloroform Bitumen A cannot reflect the presence of  $C_{14}$  hydrocarbons, making this distinction between the two indicators, and the contents of both fractions are generally lower than the actual residual oil content (Lu et al., 2012). Jarvie et al. (2007) proposed the use of the oil saturation index (OSI) to characterize the shale oil resource potential. When the OSI value of a shale oil interval is greater than 100 mg HC/g TOC, it can be considered that oil overshoot occurs. This phenomenon is favorable for shale oil intervals (Jarvie et al., 2007; Lu et al., 2012; Jarvie, 2012). The OSI has been confirmed in many shale oil resource potential evaluation studies worldwide (Lu et al., 2012; Hu et al., 2018).

As shown in Fig. 16, the correlation between  $S_1$  and TOC indicates that  $S_1$  exhibited obvious three-stage characteristics with increasing TOC: at the first stage (TOC < 0.2%),  $S_1$  slowly increased with increasing TOC, and  $S_1$  maintained a stable low value; at the second stage (0.2% < TOC < 0.8%),  $S_1$  rapidly increased with increasing TOC; and at the third stage (0.8% < TOC),  $S_1$  reached a relatively stable maximum value. According to the characteristics of the correlation between  $S_1$  and TOC, combined with the OSI oil crossing cutoff value (100 mg/g), the shale oil resources of P<sub>1</sub>f could be divided into four grades: ① enriched resources:  $S_1 > 2.2$  mg/g, OSI > 100 mg/g; ② moderately enriched resources:  $0.5 < S_1 < 2.2$  mg/g, OSI > 100 mg/g; ③ inefficient resources:  $0.5 < S_1 < 2.2$  mg/g, OSI < 100 mg/g; and ④ invalid resources:  $S_1 < 0.5$  mg/g.

According to statistics, the OSI value of the P<sub>1</sub>f shale reached 176 mg/g, far exceeding the lower benefit value of 100 mg/g, indicating that P<sub>1</sub>f exhibited a very high shale oil potential.

The shale oil potentials of the different shale lithofacies varied. The enriched resource areas all comprised felsic shale, and felsic shale was mainly distributed in the enriched and moderately enriched resource areas. Lime shale was mostly distributed in the moderately enriched and inefficient resource areas. Dolomite and mixed shale primarily occurred in the inefficient and invalid resource areas, while a small amount was observed in the moderately enriched resource areas. Felsic shale attained the highest OSI value (215 mg/g on average).

### 5.2. Controlling factors on shale oil potential

#### 5.2.1. Hydrocarbon generation potential

Rock hydrocarbon generation potential is the material basis for shale oil enrichment, when considering the influence of the hydrocarbon generation potential on the shale oil potential, the impact should be analyzed from the perspective of the organic matter abundance, organic matter type and thermal maturity (Jarvie, 2012; Fang et al., 2019; Zhang et al., 2020).

As shown in Fig. 16, the free hydrocarbon index  $S_1$  increased with increasing TOC, and when  $S_1$  gradually stabilized, TOC reached a certain value, and the generated oil was stored in the source rock and discharged into the outside environment. In this process, the organic matter abundance positively affects the shale oil potential, but the organic matter abundance does not always positively affect the shale oil potential. The felsic shale sample with an abnormally high OSI value depicted in Fig. 17a was affected by a large amount of foreign hydrocarbons. After removal, as shown in Fig. 17b, the OSI value first increased and then decreased with increasing TOC. The potential for shale oil might be significantly impacted by organic matter adsorption when TOC reaches a particular level (Hu et al., 2018; Pan et al., 2019).

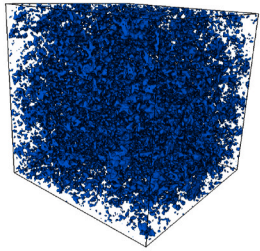
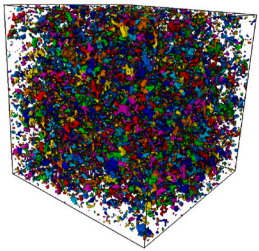
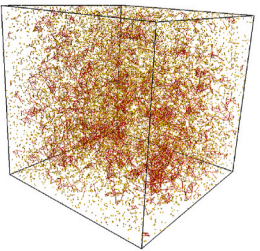
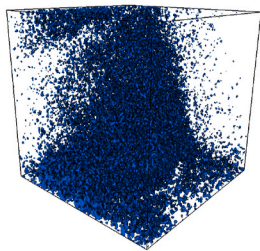
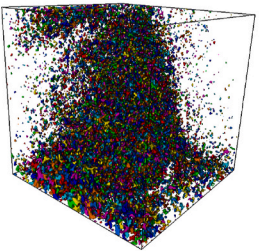
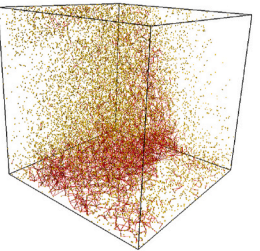
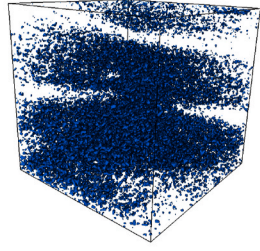
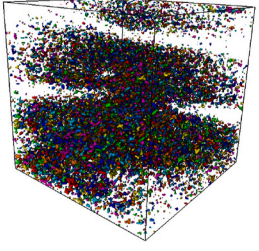
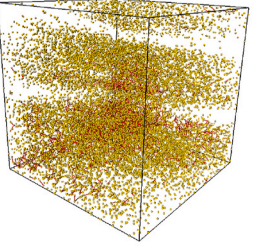
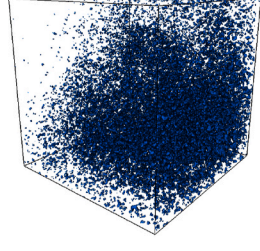
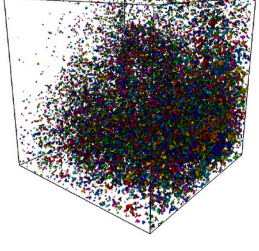
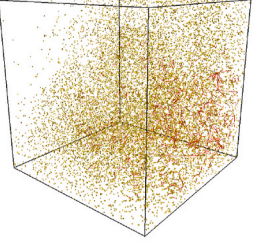
The HI can reflect the type of organic matter. As shown in Fig. 17c, the felsic shale samples with abnormally high OSI values contained a large amount of soluble organic matter that receive large amounts of foreign hydrocarbons. Among the remaining samples, as shown in Fig. 17d, the OSI value first increased and then decreased with increasing HI index value, and the maximum value was reached at HI = 430 mg HC/g rock. At a low HI index value, type 3 kerogen tends to be favored, the oil generation capacity is low, and gas is easily generated. At a high HI index value, the rock is biased toward type I kerogen, with a high hydrocarbon generation potential and notable organic matter adsorption, which can easily exert a negative impact on the shale oil potential. Type II<sub>2</sub> kerogen predominated in P<sub>1</sub>f, which is advantageous for the possibility of shale oil.

Vitrinite reflectance (Ro) was used to characterize the thermal maturity of organic matter. As shown in Fig. 17e, felsic shale in the delineated part received a large amount of foreign hydrocarbons. As shown in Fig. 17f, the OSI value first increased and then decreased with increasing Ro. Indicating that thermal maturity does not always positively influence shale oil potential and that when the appropriate thermal maturity is not reached, the shale is less capable of producing oil. When the appropriate thermal maturity is exceeded, hydrocarbon drainage occurs gradually as the organic matter evolves further, to the detriment of the shale oil resource potential. Therefore, a suitable range of thermal maturity is beneficial to shale oil potential.

#### 5.2.2. Reservoir space

The shale oil potential is closely related to the storage space, and shale oil accumulation and storage are controlled by the quality of the storage space (Liu et al., 2019a; Pan et al., 2019). Large pores and fractures play a dominant role in shale oil storage and connectivity (Ning et al., 2017; Yu et al., 2018a), and shale oil can exist in three states in micro/nanopores and fractures: adsorption, dissolved and free states. Free oil is the most favorable state for the economic recovery of shale oil,



Lithofacies	Pore model	Pore connectivity model	Pore ball and stick model
Felsic shale			
Lime shale			
Dolomitic shale			
Mixed shale			

Note: Pore model (blue represents pore space), pore connectivity model (each color represents a connected pore network), pore ball-and-stick model (yellow balls represent pores, red sticks represent throats connected to pores), model Specification 1368\*1368\*1368 $\mu\text{m}$

Fig. 14. Micro-CT scan images of different lithofacies.

and free oil mainly occurs in large pores and fractures. The shale oil potential is not favored by the adsorbed and dissolved oil states, which are mostly found on the surface of minerals and inside organic matter (Jarvie, 2012; Jarvie et al., 2007; Li et al., 2016c; Li et al., 2019b). As shown in Fig. 18, The OSI value showed a positive association with both meso- and macropores and a negative correlation with micropores. This indicates that pores within the different size ranges impose different effects on the shale oil content. Micropores exhibit a large specific

surface area, and as the storage space for smaller hydrocarbon molecules, micropores mainly store adsorbed oil, which is not conducive to the shale oil potential. In contrast, large pores such as meso- and macropores may host free oil, which positively contributes to the oil-bearing property of shale. The size of the reservoir space is a key element impacting the shale potential, as shown by the positive association between the shale oil potential OSI and mercury porosity.

**Table 2**

Characteristics of pore structure parameters of micro-CT of different lithofacies.

Lithofacies	Depth/ m	Number of pore	Number of throat	pore diameter/ μm	Throat diameter/ μm	length of throat/μm	Pore coordination number	$\Phi_{CT}/\%$
Felsic shale	4910.63	20,844	13,484	9.88	6.99	34.02	1.3 ( 0–24 )	7.50
Lime shale	4694.31	15,373	8896	9.20	7.27	42.62	1.1 ( 0–34 )	5.70
Dolomitic shale	4594.63	18,098	8263	8.60	5.90	33.10	0.9 ( 0–29 )	4.60
Mixed shale	3955.58	16,407	2409	6.70	3.77	29.93	0.29 ( 0–11 )	2.10

Note: 1.3 (0–24) stands for Ave. (Min.-Max.).

**Table 3**Hydrocarbon migration parameters of P<sub>1</sub>f shale.

Well	Sample no.	Depth/m	Lithofacies	TOC/%	S <sub>1</sub>	OSI	Ro/%	HCGR	HCGQ	$\Delta S_1$
MY1	M-34	4779.67	felsic shale	1.58	0.39	24.64	1.38	244.73	3.87	3.48
MY1	M-35	4781.65	felsic shale	1.29	0.30	23.29	1.38	164.58	2.12	1.82
FN2	M-99	4041.80	dolomitic shale	2.95	0.91	30.82	1.04	278.90	8.24	7.33
FN14	M-101	4166.05	dolomitic shale	2.06	1.28	62.29	1.09	194.28	3.99	2.71
MY1	M-84	4770.42	dolomitic shale	1.24	1.03	83.00	1.38	243.97	3.03	2.00
MY1	M-86	4776.22	dolomitic shale	1.52	0.23	15.15	1.38	244.45	3.71	3.48
FN1	M-103	4340.00	dolomitic shale	2.31	0.39	16.89	1.17	312.54	7.22	6.83
MY1	M-2	4590.89	felsic shale	0.60	2.00	331.29	1.29	154.48	0.93	−1.07
MY1	M-8	4612.33	felsic shale	0.25	2.46	1004.08	1.30	343.74	0.84	−1.62
MY1	M-11	4625.16	felsic shale	0.25	3.16	1267.55	1.30	345.21	0.86	−2.30
MY1	M-25	4707.01	felsic shale	1.11	3.50	314.75	1.35	160.64	1.79	−1.71
MY1	M-29	4738.13	felsic shale	0.41	2.00	484.50	1.36	84.82	0.35	−1.65
MY1	M-32	4750.05	felsic shale	0.91	2.79	307.74	1.37	162.91	1.48	−1.31
MY1	M-33	4768.12	felsic shale	1.36	3.45	253.12	1.38	163.87	2.23	−1.22
MY1	M-47	4750.82	felsic shale	1.25	3.18	253.79	1.37	162.95	2.04	−1.14
MY1	M-57	4708.88	felsic shale	0.77	3.21	418.90	1.35	160.74	1.23	−1.98
MY1	M-67	4910.63	felsic shale	1.36	8.39	618.73	1.45	171.31	2.32	−6.07
MY1	M-68	4886.00	felsic shale	0.98	5.65	575.65	1.44	170.03	1.67	−3.98
MY1	M-69	4886.38	felsic shale	0.71	4.71	660.50	1.44	170.05	1.21	−3.50
MY1	M-70	4891.04	felsic shale	1.17	7.05	603.60	1.44	170.29	1.99	−5.06
MY1	M-71	4911.77	felsic shale	1.00	6.91	688.25	1.45	171.37	1.72	−5.19
MY1	M-139	4714.99	lime shale	0.65	2.78	431.01	1.35	239.42	0.90	−1.88
FN2	M-147	4100.58	lime shale	1.57	4.26	271.34	1.07	188.95	2.97	−1.29

Note: HCGR: hydrocarbon generation rate; HCGQ: hydrocarbon generation quantity,  $HCGQ = HCGR \times TOC$ ;  $\Delta S_1 = HCGQ - S_1$ ; The unit of  $S_1$ ,  $\Delta S_1$  and HCGQ are mg HC/g Rock; The units of OSI, HI and HCGR are mg HC/g TOC; data from partial samples.

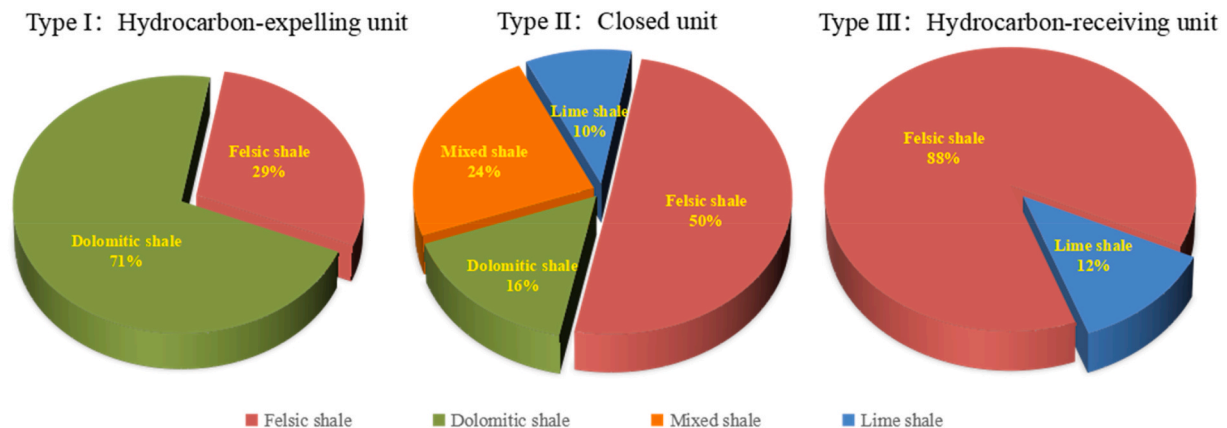
**Table 4**

Hydrocarbon migration unit division.

Unit type	$\Delta S_1$ (mg HC/g Rock)	State of hydrocarbon migration
Type I : Hydrocarbon-expelling unit	$\Delta S_1 > 1$	A lot of hydrocarbons is expelled
Type II : Closed unit	$1 > \Delta S_1 > -1$	Poor flow of hydrocarbons
Type III : Hydrocarbon-receiving unit	$\Delta S_1 < -1$	Accept more foreign hydrocarbons

### 5.2.3. Hydrocarbon migration

Hydrocarbon migration within the shale system can indicate the retention, discharge and accumulation of shale oil, which directly affects the enrichment of shale oil. (Han et al., 2019; Chen et al., 2020). Considering that  $\Delta S_1$  can characterize the hydrocarbon expulsion and migration state in shale units,  $S_1$  has continued to be a crucial criterion for assessing shale oil content, and the OSI is a recognized parameter in the assessment of shale oil content and shale oil potential (Jarvie, 2012; Hu et al., 2018). As shown in Fig. 19,  $\Delta S_1$  is negatively correlated with  $S_1$  and OSI, and the capillary pressure difference resulting from the difference in pore throat size between shale intervals may represent the

**Fig. 15.** Migration status of hydrocarbons in different lithofacies shale.

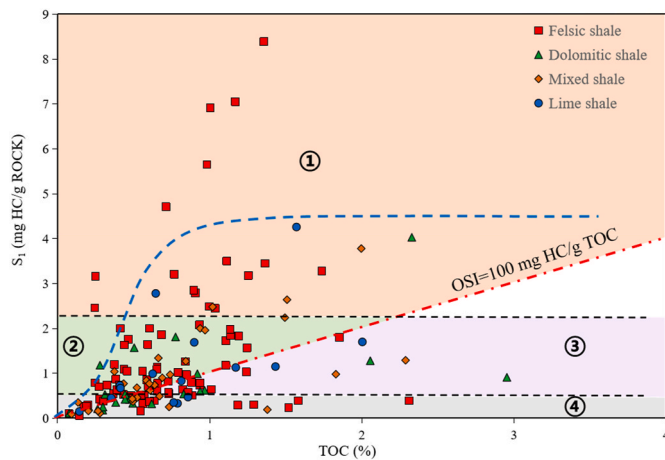


Fig. 16. Evaluation map of shale oil potential of P<sub>1f</sub>.

main driving force of hydrocarbon migration (Chen et al., 2019), indicating that hydrocarbon migration greatly influences the shale oil potential. The shale oil potential of shale formations exhibiting hydrocarbon expulsion is low, while the shale oil potential of shale formations contributing to hydrocarbon migration is high.

### 5.3. Shale oil enrichment model of different lithofacies

The hydrocarbon generation capacity constitutes the material basis of the shale oil potential, and the storage capacity controls the size of the shale oil storage space. Hydrocarbon migration is highly important for shale oil enrichment (Liu et al., 2019a; Han et al., 2019; Zhang et al., 2020; Chen et al., 2021). Therefore, the generation, storage, and migration of shale hydrocarbons determine the potential for shale oil. The different lithofacies exhibited varying hydrocarbon generation, storage capacity and micromigration characteristics.

Felsic shale shows a good hydrocarbon generation potential. Most of the pores included large-diameter matrix pores and microfractures. Macroscopically, high-angle fractures could also be observed. CT scanning revealed that felsic shale exhibited a satisfactory porosity and connectivity, which is favorable for oil and gas accumulation and

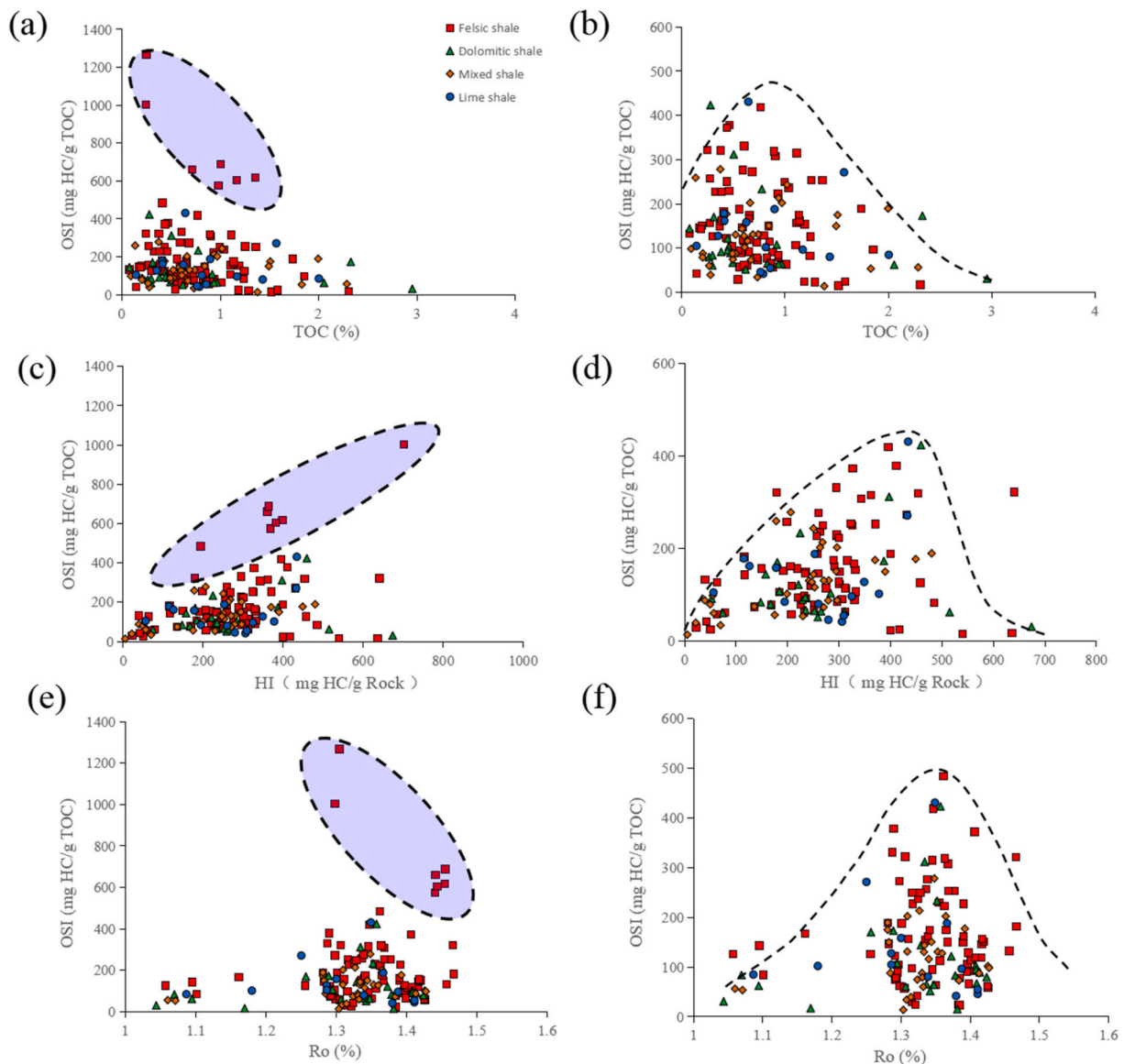


Fig. 17. Effect of hydrocarbon generation potential on shale oil potential.

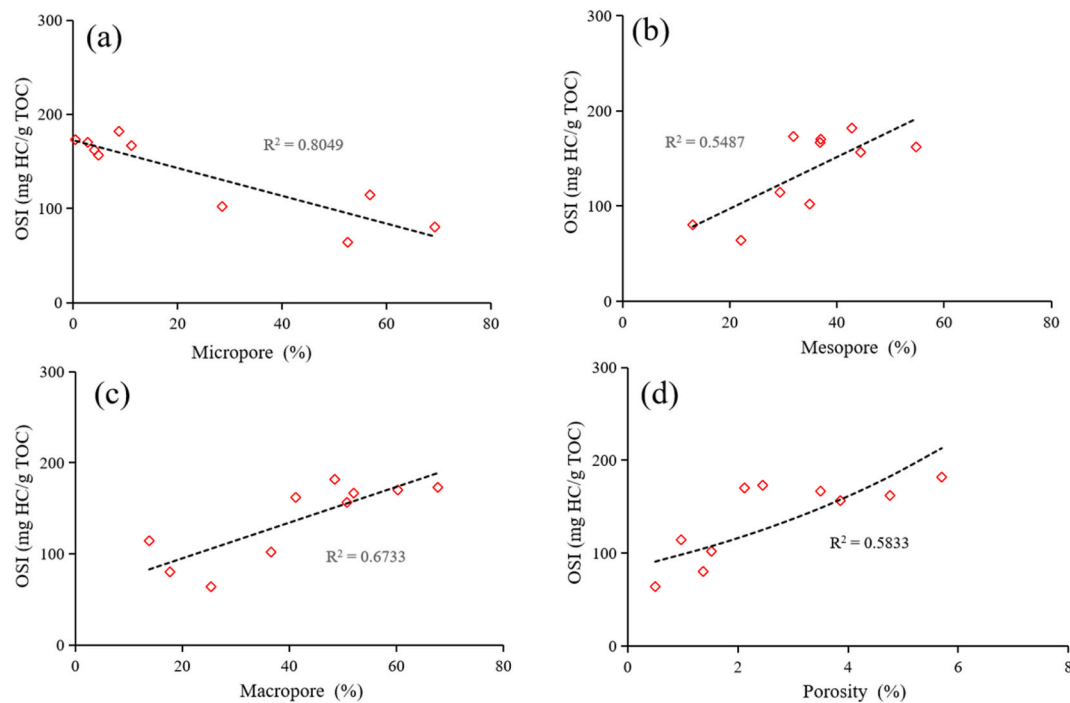


Fig. 18. Relationship between pore parameters and shale oil potential.

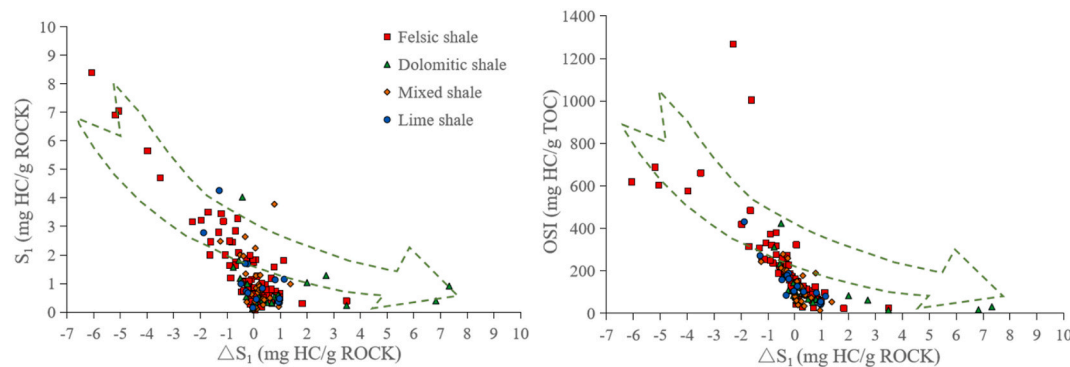


Fig. 19. Relationship between hydrocarbon migration and shale oil potential.

migration.  $\Delta S_1$  demonstrated that felsic shale achieved a high ability to receive foreign hydrocarbons. Previous research has indicated that the brittleness of rock is related to the mineral composition, and the higher brittle mineral index value of felsic shale is beneficial to later fracture production. Therefore, felsic shale contains shale oil comprising not only migrated foreign hydrocarbons but also self-enriched shale oil.

Dolomite shale attained a high hydrocarbon generation capacity but a low storage capacity.  $\Delta S_1$  revealed that dolomitic shale exhibited a notable hydrocarbon expulsion capacity, indicating that dolomitic shale is biased toward source rocks. Moreover, dolomite shale contained laminar sedimentary structures, and microfractures between laminae facilitated oil and gas migration. Therefore, Dolomite shale with high hydrocarbon production capacity, high outgassing capacity and poor storage capacity resulting in low oil content.

Lime shale achieved a weak hydrocarbon generation capacity and high storage capacity, more favorable to good reservoirs than dolomitic shale.  $\Delta S_1$  indicated that the lime shale has a strong hydrocarbon accepting capacity second only to the felsic shale and can be a high quality reservoir.

Mixed shale exhibited the lowest hydrocarbon generation capacity, low porosity and connectivity, as revealed via CT scanning, lack of

fractures and low reservoir capacity. Tight reservoir characteristics are not conducive to oil and gas accumulation and migration.  $\Delta S_1$  demonstrated that mixed shale was a closed unit without hydrocarbon migration, with self-generation and self-accumulation features. Therefore, the shale oil potential of mixed shale was low, which did not favor the development of shale oil.

According to the enrichment characteristics of shale oil in the four lithofacies, shale oil enrichment models of the different lithofacies were established (Fig. 20). Felsic shale is an enriched oil shale with a high hydrocarbon generation potential and high storage capacity that can accept foreign hydrocarbons. Mixed shale is a self-generating and self-accumulating oil shale with a low hydrocarbon production capacity and low storage capacity. Lime shale is a partial reservoir-type oil shale with a low hydrocarbon production capacity and satisfactory storage capacity that can receive foreign hydrocarbons. Dolomite shale is a partial source rock-type oil shale exhibiting a high hydrocarbon generation capacity and low storage capacity, which can expel hydrocarbons. In summary, felsic shale realizes the characteristics of a high hydrocarbon generation potential, notable storage capacity, suitable pore connectivity, ease of foreign hydrocarbon migration, high content of brittle minerals and easy fracture production. Felsic shale is the most



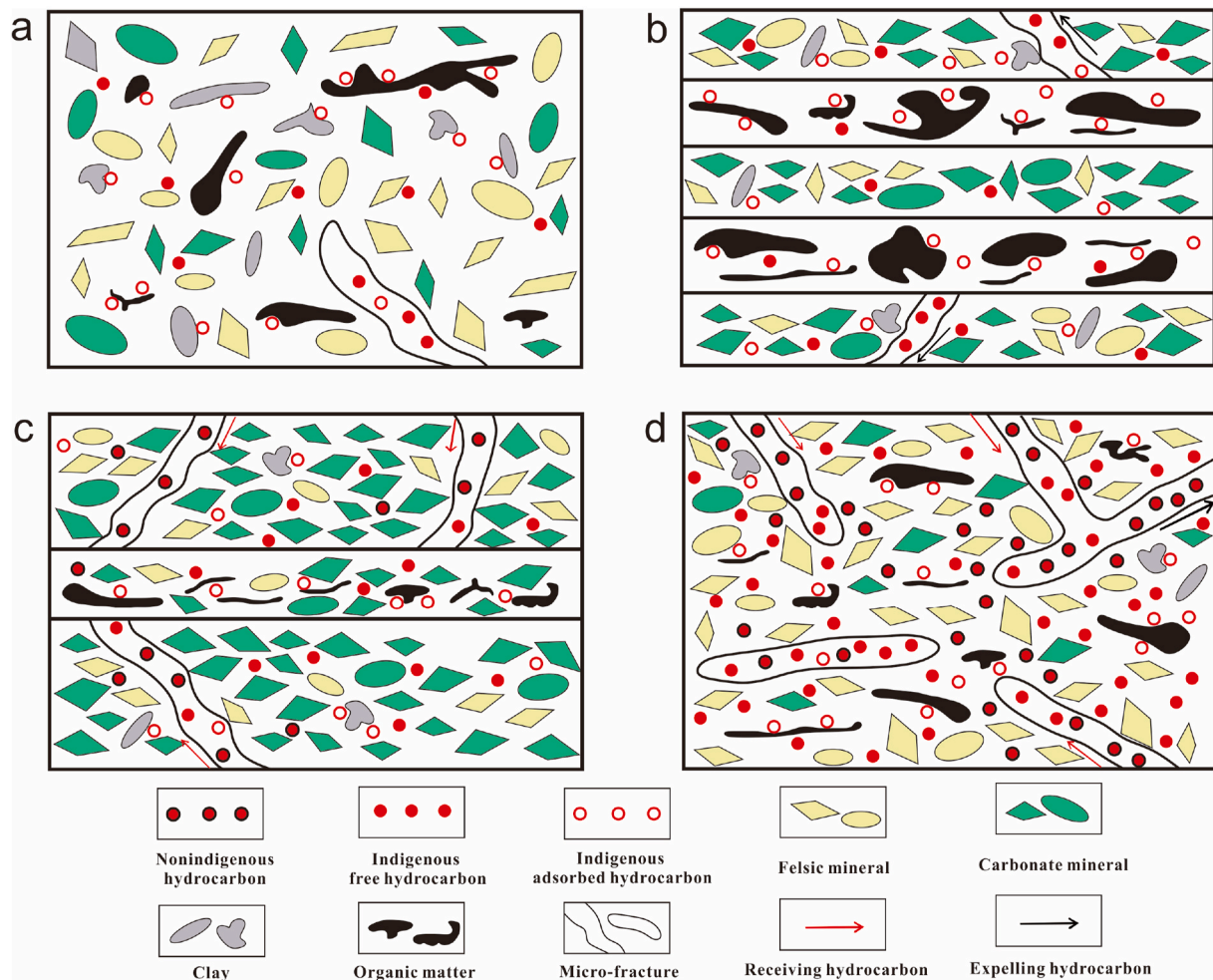


Fig. 20. Shale oil enrichment patterns of different lithofacies (a: mixed shale b: dolomitic shale c: lime shale d: felsic shale).

favorable exploration target in P<sub>1</sub>f within the Mahu Sag.

## 6. Conclusions

Understanding the role of complex rocks in controlling the shale oil potential is important for the development of shale oil reservoirs. In this paper, experiments related to organic geochemistry and storage space research were used to evaluate the shale oil potential of the ancient alkaline lacustrine P<sub>1</sub>f formation from the three aspects of source, storage and transportation, reveal the control of complex lithofacies on the shale oil potential and establish a model of shale oil enrichment for the different lithofacies. Research shows the P<sub>1</sub>f is complex in lithology and could be divided into four types of lithofacies according to the mineralogy: felsic, dolomitic, lime and mixed shale types. Geochemical characteristics indicated that the shale TOC distribution ranged from 0.12% to 2.91% (average: 1.02%), with type II<sub>2</sub> kerogen dominating over type II<sub>1</sub> kerogen, while Ro indicated that the shale had reached the mature and high-maturity stages and occurred at peak oil production. The felsic and dolomitic shale types attained a high hydrocarbon generation potential. The P<sub>1</sub>f shale mainly contained inorganic mineral pores and microfractures but not organic pores. Large-sized intergranular pores, dissolution pores and widely developed microfractures are the most favorable storage spaces in shale, which are favorable for oil and gas migration and accumulation. Felsic shale with high-angle fractures and lime shale with large-scale dissolution pores were favorable shale oil reservoirs, with a suitable reservoir space, pore structure and pore connectivity.

The OSI value of the P<sub>1</sub>f shale could reach 176 mg HC/g TOC, far exceeding the lower benefit limit of 100 mg HC/g TOC, indicating a satisfactory shale oil potential. The shale oil potential is controlled by hydrocarbon generation, storage capacity and hydrocarbon migration, and the various lithofacies differed in various aspects. Felsic shale is an enriched oil shale with a high hydrocarbon generation potential and high storage capacity that can receive foreign hydrocarbons. Mixed shale is a self-generating and self-accumulating oil shale with a low hydrocarbon production capacity and low storage capacity. Lime shale is a partial reservoir-type oil shale with a low hydrocarbon production capacity and satisfactory storage capacity that can receive foreign hydrocarbons. Dolomite shale is a partial source rock-type oil shale exhibiting a high hydrocarbon generation capacity and low storage capacity, which can expel hydrocarbons. Among these lithofacies types, felsic shale, as an enriched oil shale, exhibited the characteristics of a high hydrocarbon generation potential, notable storage capacity, suitable pore connectivity, ease of foreign hydrocarbon migration, high content of brittle minerals and ease of fracture production. This lithofacies is the most favorable exploration target in P<sub>1</sub>f within the Mahu Sag.

## Credit authors statement

Jiahao Lv: Conceptualization, Methodology, Software, Writing-Original draft preparation. Fujie Jiang: Supervision. Tao Hu: Review & Editing. Chenxi Zhang: Validation. Renda Huang: Validation. Meiling Hu: Data curation. Jing Xue: Data curation. Liliang Huang: Supervision.

Yuping Wu: Investigation.

## Declaration of competing interest

The authors declare that they have no known competing financial interests or personal relationships that could have appeared to influence the work reported in this paper.

## Data availability

Data will be made available on request.

## Acknowledgments

This study is supported by the National Natural Science Foundation of China (41872128, 42202133), the Strategic Cooperation Technology Projects of CNPC and CUPB (ZLZX2020-01-05). We are grateful to the Xinjiang Oilfield for the support and help with experiments and basic data.

## Appendix A. Supplementary data

Supplementary data to this article can be found online at <https://doi.org/10.1016/j.geoen.2023.211501>.

## References

- Barker, C., 1974. Pyrolysis techniques for source-rock evaluation. *Am. Assoc. Petrol. Geol. Bull.* 58, 2349–2361.
- Cao, J., Xia, L.W., Wang, T.T., Zhi, D.M., Tang, Y., Li, W.W., 2020. An alkaline lake in the Late Paleozoic Ice Age (LPIA): a review and new insights into paleoenvironment and petroleum geology. *Earth Sci. Rev.* 202, 103091.
- Chalmers, G.R., Bustin, R.M., Power, I.M., 2012. Characterization of gas shale pore systems by porosimetry, pycnometry, surface area, and field emission scanning electron microscopy/transmission electron microscopy image analyses: examples from the Barnett, Woodford, Haynesville, Marcellus, and Doig units. *AAPG (Am. Assoc. Pet. Geol.) Bull.* 96, 1099–1119.
- Chen, Y., Lin, S., Bai, B., Zhang, T., Hu, S., 2020. Effects of petroleum retention and migration within the Triassic chang 7 member of the ordos basin, China. *Int. J. Coal Geol.* 225, 103502.
- Chen, D., Pang, X., Jiang, F., Liu, G., Liu, Y., 2021. Shale oil potential and mobility of low-maturity lacustrine shales: implications from NMR analysis in the Bohai bay basin. *Energy Fuel.* 35 (3).
- Chen, L., Jiang, Z., Liu, K., Wang, P., Ji, W., Gao, F., Li, P., Hu, T., Zhang, B., Huang, H., 2016. Effect of lithofacies on gas storage capacity of marine and continental shales in the Sichuan Basin, China. *J. Nat. Gas Sci. Eng.* 36, 773–785.
- Chao, L., Cao, Y., Jiang, Z., Wu, J., Song, G., Wang, Y., 2017. Shale oil potential of lacustrine black shale in the Eocene Dongying depression: Implications for geochemistry and reservoir characteristics. *AAPG Bulletin* 101 (11), 1835–1858.
- Chen, Z., Jiang, W., 2018. Organic matter, mineral composition, pore size, and gas sorption capacity of lacustrine mudstones: implications for the shale oil and gas exploration in the Dongying Depression, eastern China. *AAPG (Am. Assoc. Pet. Geol.) Bull.* 102 (8), 1565–1600.
- Curtis, M.E., Cardott, B.J., Sondergeld, C.H., Rai, C.S., 2012. Development of organic porosity in the Woodford Shale with increasing thermal maturity. *Int. J. Coal Geol.* 103, 26–31.
- EIA, 2014. Shale Oil and Shale Gas Resources Are Globally Abundant. U.S. Energy Information Administration.
- Espitalié, J., Laporte, L.J., Madec, M., Marquis, F., Leplat, P., Paulet, J., 1977. Méthode rapide caractérisation des roches mères de leur potentiel pétrolier et de leur degré d'évolution. *Rev. Inst. Franc. Petrol.* 32, 23–42.
- Fang, R., Littke, R., Zieger, L., Baniasad, A., Li, M., Schwarzbauer, J., 2019. Changes of composition and content of tricyclic terpene, hopane, sterane, and aromatic biomarkers throughout the oil window: a detailed study on maturity parameters of Lower Toarcian Posidonia Shale of the Hils Syncline, NW Germany. *Org. Geochem.* 103928.
- Feng, C., Li, T., He, W., Zheng, M., 2020. Organic geochemical traits and paleo-depositional conditions of source rocks from the carboniferous to permian sediments of the northern mahu sag, Junggar Basin, China. *J. Petrol. Sci. Eng.* 191, 107–117.
- Hakimi, M.H., Abdullah, W.H., Alqudah, M., Makeen, Y.M., Mustapha, K.A., 2016. Organic geochemical and petrographic characteristics of the oil shales in the Lajjun area, Central Jordan: origin of organic matter input and preservation conditions. *Fuel* 181, 34–45.
- Han, Y., Horsfield, B., Mahlstedt, N., Wirth, R., Lareau, H., 2019. Factors controlling source and reservoir characteristics in the Niobrara shale oil system, Denver basin. *AAPG (Am. Assoc. Pet. Geol.) Bull.* 103 (9), 2045–2072.
- He, D., Wu, S., Zhao, L., Zheng, M., Li, D., Lu, Y., 2018. Tectono-depositional setting and its evolution during Permian to triassic around Mahu sag, Junggar Basin. *Xinjing Pet. Geol.* 39, 35–47 (in Chinese with English abstract).
- Hu, T., Pang, X., Shu, J., Wang, Q., Hui, L., 2018. Oil content evaluation of lacustrine organic-rich shale with strong heterogeneity: a case study of the Middle Permian Lucaogou Formation in Jimusaer Sag, Junggar Basin, NW China. *Fuel* 221, 196–205.
- Hutton, A., 1994. Chemical and petrographic classification of kerogen/macerals. *Energy Fuel.* 8, 1478–1488.
- Jarvie, D.M., 2012. Shale resource systems for oil and gas: Part 2–Shale oil resource systems. In: Breyer, J.A. (Ed.), *Shale Reservoirs—Giant Resources for the 21st Century*, vol. 97. Am. Assoc. Pet. Geol. Bull., pp. 89–119.
- Jarvie, D.M., Hill, R.J., Ruble, T.E., Pollastro, R.M., 2007. Unconventional shale-gas systems: the Mississippian Barnett Shale of north-central Texas as one model for thermogenic shale-gas assessment. *AAPG (Am. Assoc. Pet. Geol.) Bull.* 91, 475–499.
- Jiang, Z.X., Liang, C., Wu, J., Zhang, J.G., Zhang, W.Z., Wang, Y.S., Liu, H.M., Chen, X., 2013. Several issues in sedimentological studies on hydrocarbon-bearing fine-grained sedimentary rocks. *Acta Pet. Sin.* 34 (6), 1031–1039 (in Chinese with English abstract).
- Katz, B.J., Lin, F., 2021. Consideration of the limitations of thermal maturity with respect to vitrinite reflectance, Tmax, and other proxies. *AAPG (Am. Assoc. Pet. Geol.) Bull.* 105, 695–720.
- Kruger, M.A., 1983. Diagenesis of miocene biogenic sediments in Lost Hills oil field, San Joaquin basin, California. In: Isaacs, C.M., Garrison, R.E. (Eds.), *Petroleum Generation and Occurrence in the Miocene Monterey Formation*. SEPMP, California: Los Angeles, California, Pacific Section, pp. 39–51.
- Langford, F.F., Blanc-Valleron, M.M., 1990. Interpreting Rock-Eval pyrolysis data using graphs of pyrolyzable hydrocarbons vs. total organic carbon (1). *AAPG Bull.* 74, 799–804.
- Li, C., Kong, L., Ostadhasan, M., Gentzis, T., 2019a. Nanoscale pore structure characterization of tight oil formation: a case study of the Bakken Formation. *Energy Fuel.* 33 (7), 6008–6019.
- Li, W., Cao, J., Zhi, D., Tang, Y., He, W., Wang, T., Xia, L., 2021. Controls on shale oil accumulation in alkaline lacustrine settings: late Paleozoic Fengcheng Formation, northwestern Junggar Basin. *Mar. Petrol. Geol.* 129, 105107.
- Li, M., Chen, Z., Ma, X., 2019b. Shale oil resource potential and oil mobility characteristics of the eocene-Oligocene Shahejie Formation, Jiyang Super-depression, Bohai Bay Basin of China. *Int. J. Coal Geol.* 204 (14), 130–143.
- Li, S., Hu, S., Xie, X., 2016a. Assessment of shale oil potential using a new free hydrocarbon index. *Int. J. Coal Geol.* 156, 74–85.
- Li, D., He, D., Tang, Y., 2016b. Reconstructing multiple arc-basin systems in the Altai–Junggar area (NW China): implications for the architecture and evolution of the western Central Asian Orogenic Belt. *Asian Earth Sci.* 121, 84–107.
- Li, Z., Zou, Y.R., Xu, X.Y., Sun, J.N., Li, M.W., Peng, P.A., 2016c. Adsorption of mudstone source rock for shale oil - experiments, model and a case study. *Org. Geochem.* 92, 55–62.
- Liu, B., Shi, J., Xiaofei, Fu, Yanfang, L., Sun, X., Gong, L., 2018. Petrological characteristics and shale oil enrichment of lacustrine fine-grained sedimentary system: a case study of organic-rich shale in first member of Cretaceous Qingshankou Formation in Gulong Sag, Songliao Basin, NE China[J]. *Petrol. Explor. Dev.* 45 (5), 11.
- Liu, B., Wang, H., Fu, X., 2019a. Lithofacies and depositional setting of a highly prospective lacustrine shale oil succession from the Upper Cretaceous Qingshankou Formation in the Gulong sag, northern Songliao Basin, northeast China. *AAPG (Am. Assoc. Pet. Geol.) Bull.* 103 (2), 405–432.
- Liu, B., Schieber, J., Mastalerz, M., 2017a. Combined SEM and reflected light petrography of organic matter in the New Albany Shale (Devonian-Mississippian) in the Illinois Basin: a perspective on organic pore development with thermal maturation. *Int. J. Coal Geol.* 184, 57–72.
- Liu, K., Ostadhasan, M., Jie, Z., Gentzis, T., Rezaee, R., 2017b. Nanoscale pore structure characterization of the bakken shale in the USA. *Fuel* 209, 567–578.
- Liu, K., Ostadhasan, M., Sun, L., Zou, J., Yuan, Y., Gentzis, T., Zhang, Y., Carvajal-Ortiz, H., Rezaee, R.A., 2019b. A comprehensive pore structure study of the Bakken Shale with SANS, N<sub>2</sub> adsorption and mercury intrusion. *Fuel* 245, 274–285.
- Loucks, R.G., Ruppel, S.C., 2007. Mississippian Barnett shale: lithofacies and depositional setting of a deepwater shale-gas succession in the Fort Worth Basin, Texas. *AAPG (Am. Assoc. Pet. Geol.) Bull.* 91 (4), 579–601.
- Lu, S.F., Huang, W.B., Chen, F.W., 2012. Classification and evaluation criteria of shale oil and gas resources: discussion and application. *Petrol. Explor. Dev.* 39 (2), 249–256 (in Chinese).
- Mccarthy, K., Rojas, K., Niemann, M., Palmowski, D., Peters, K., Stankiewicz, A., 2011. Basic petroleum geochemistry for source rock evaluation. *Oilfield Rev.* 23, 32–43.
- Mohialdeen, I.M.J., Hakimi, M.H., 2016. Geochemical characterisation of Tithonian–Berriasian Chia Gara organic-rich rocks in northern Iraq with an emphasis on organic matter enrichment and the relationship to the bioproductivity and anoxia conditions. *J. Asian Earth Sci.* 116, 181–197.
- Nie, H.K., Zhang, P.X., Bian, R.K., 2016. Oil accumulation characteristics of China continental shale. *Earth Sci. Front.* 23 (2), 55–62.
- Ning, C., Jiang, Z., Gao, Z., Su, S., Li, T., Wang, G., 2017. Characteristics and controlling factors of reservoir space of mudstone and shale in es3x in the zhanhua sag. *Mar. Petrol. Geol.* 11, 214–224.
- Pan, Y.H., Li, M.W., Sun, Y.G., Li, Z.M., Peng Liu, P., Bin Jiang, B., Liao, Y.H., 2019. Characterization of free and bound bitumen fractions in a thermal maturation shale sequence. Part 1: acidic and neutral compounds by negative-ion ESI-FT-ICR MS. *Org. Geochem.* 134, 1–15.

- Peng, N., He, S., Hu, Q., Zhang, B., He, X., Zhai, G., He, C., Yang, R., 2019. Organic nanopore structure and fractal characteristics of Wufeng and lower member of Longmaxi shales in southeastern Sichuan, China. *Mar. Petrol. Geol.* 103, 456–472.
- Peters, K., Cassa, M., 1994. Applied source rock geochemistry. In: Magoon, L.B., Dow, W. G. (Eds.), *The Petroleum System from Source to Trap*, vol. 60. AAPG Memoir, pp. 93–117.
- Peters, K.E., Hackley, P.C., Thomas, J.J., Pomerantz, A.E., 2018. Suppression of vitrinite reflectance by bitumen generated from liptinite during hydrous pyrolysis of artificial source rock. *Org. Geochem.* 125, 220–228.
- Scott, A., 2002. Coal petrology and the origin of coal macerals: a way ahead? *Int. J. Coal Geol.* 50, 119–134.
- Sing, K.S.W., Everett, D.H., Haul, R.A.W., 1985. Reporting physic-sorption data for gas/solid systems with special reference to the determination of surface area and porosity. *Pure Appl. Chem.* 57 (4), 603–619.
- Singh, P., Slatt, R., Borges, G., Perez, R., Coffey, W., 2009. Reservoir Characterization of Unconventional Gas Shale Reservoirs: Example from the Barnett Shale (Texas, U.S. A).
- Tang, Y., He, W., Bai, Y., Zhang, X., Wu, W., 2021. Source rock evaluation and hydrocarbon generation model of a permian alkaline lakes—a case study of the fengcheng formation in the mahu sag, junggar basin. *Minerals* 11 (6), 644.
- Tao, S., Wang, Y., Tang, D., Wu, D., Xu, H., He, W., 2012. Organic petrology of fukang permian Lucaogou formation oil shales at the northern foot of bogda mountain, Junggar Basin, China. *Int. J. Coal Geol.* 99, 27–34.
- Tian, H., Pan, L., Xiao, X.M., 2013. A preliminary study on the pore characterization of Lower Silurian black shales in the Chuandong Thrust Fold Belt, southwestern China using low pressure N<sub>2</sub> adsorption and FE-SEM methods. *Mar. Petrol. Geol.* 48, 8–19.
- Tissot, B., Welte, D.H., 1984. *Petroleum Formation and Occurrence*. Springer, Berlin.
- Wang, T., Cao, J., Jin, J., Xia, L., He, W., 2020a. Spatiotemporal Evolution of a Late Paleozoic Alkaline Lake in the Junggar Basin, China. *Marine and Petroleum Geology*, 104799.
- Wang, X., Liu, L., Wang, Y., Sheng, Y., Luo, Z., 2020b. Comparison of the pore structures of lower silurian longmaxi formation shales with different lithofacies in the southern sichuan basin, China. *J. Nat. Gas Sci. Eng.* 81, 103419.
- Wang, G., 2012. Laminar combination and genetic classification of eogene shale in Jiyang depression. *J. Jilin Univ. (Earth Sci. Ed.)* 42 (3), 666–671.
- Xie, X., Li, M., Littke, R., Huang, Z., Ma, X., Jiang, Q., Snowdon, L., 2016. Petrographic and geochemical characterization of microfacies in a lacustrine shale oil system in the Dongying Sag, Jiyang Depression, Bohai Bay Basin, eastern China. *Int. J. Coal Geol.* 165, 49–63.
- Yu, K., Cao, Y., Qiu, L., Sun, P., 2018a. The hydrocarbon generation potential and migration in an alkaline evaporite basin: the early permian fengcheng formation in the junggar basin, northwestern China. *Mar. Petrol. Geol.* 98, 12–32.
- Yu, K., Cao, Y., Qiu, L., Sun, P., 2019. Depositional environments in an arid, closed basin and their implications for oil and gas exploration: The lower Permian Fengcheng Formation in the Junggar Basin, China. *AAPG Bulletin* 103 (9), 2073–2115.
- Yu, K., Cao, Y., Qiu, L., Sun, P., Jia, X., Wan, M., 2018b. Geochemical characteristics and origin of sodium carbonates in a closed alkaline basin: the lower permian Fengcheng Formation in the mahu sag, northwestern Junggar Basin, China. *Palaeogeogr. Palaeoclimatol. Palaeoecol.* 511, 506–531.
- Zeng, W., Zhou, G., Cao, T., Song, Z., 2021. Pore Structure of the Cretaceous Lacustrine Shales and Shale-Oil Potential Assessment in the Songliao Basin, Northeast china.
- Zhang, P., Xu, Y., Meng, Q., Liu, Z., Zhang, J., Shen, L., Zhang, S., 2020. Sequence stratigraphy and geochemistry of oil shale deposits in the upper cretaceous qingshankou formation of the Songliao Basin, NE China: implications for the geological optimization of in situ oil shale conversion processing. *Energies* 13, 2964.
- Zhang, Z., Yuan, X., Wang, M., Zhou, C., Tang, Y., Chen, X., Lin, M., Cheng, D., 2018. Alkaline-lacustrine deposition and paleoenvironmental evolution in permian Fengcheng Formation at the mahu sag, Junggar Basin, NW China. *Petrol. Explor. Dev.* 45, 1036–1049.
- Zhi, D.M., Tang, Y., He, W.J., Guo, X., Zheng, M., Huang, L., 2021. Orderly coexistence and accumulation models of conventional and unconventional hydrocarbons in lower permian Fengcheng Formation, mahu sag, Junggar Basin. *Petrol. Explor. Dev.* 48 (1), 1–14.
- Zou, C., Pan, S., Horsfield, B., Yang, Z., Zhang, L., 2019. Oil retention and intrasource migration in the organic-rich lacustrine chang 7 shale of the upper triassic yanchang formation, ordos basin, central China. *AAPG (Am. Assoc. Pet. Geol.) Bull.* 103 (11), 2627–2663.
- Zou, C., Yang, Z., Cui, J., Zhu, R., Hou, L., Tao, S., 2013. Formation mechanism, geological characteristics and development strategy of nonmarine shale oil in China. *Petrol. Explor. Dev.* 40 (1), 15–27.
- Zou, Y., Sun, J., Li, Z., Xu, X., Li, M., Peng, P., 2018. Evaluating shale oil in the Dongying Depression, Bohai Bay Basin, China, using the oversaturation zone method. *J. Petrol. Sci. Eng.* 161, 291–301.